



University of Padova

Department of Management and Engineering

Product Innovation Engineering

Master Thesis

Multiaxial low cycle fatigue behavior of notched components under non proportional loading

Candidate: Stefano Bressan

Advisor: Ch.mo Prof. Filippo Berto

Co-Advisors: Dr. Pasquale Gallo,

Prof. Takamoto Itoh

Academic Year 2015/2016



Università degli studi di Padova

Dipartimento di tecnica e gestione dei sistemi industriali

Corso di laurea in ingegneria dell'innovazione del prodotto

Tesi di laurea magistrale

**Fatica a basso numero di cicli di componenti
intagliati in presenza di sollecitazioni non
proporzionali**

Laureando: Stefano Bressan

Relatore: Ch.mo Prof. Filippo Berto

Correlatori: Dr. Pasquale Gallo

Prof. Takamoto Itoh

Anno Accademico 2015/2016

SUMMARY

The aim of the present work is to create a finite element model of notched specimens made of stainless steel 316L type which undergoes multiaxial low cycle fatigue with non-proportional loading. The modeled and analyzed specimens have been already tested in a previous work by Itoh *et al.* [20] with a strain controlled multiaxial fatigue test, which aim was to find a relation between fatigue life and the strain parameter. This relation has been described with a model which takes into account additional hardening due to non proportional loading and the intensity of the load cycle. Both parameters modify the nominal strain, which has been correlated to the number of cycles to failure. This model was originally defined and applied for smooth specimens, giving good results. Successively, the model has been modified to take into account the stress concentration factor due to the presence of a notch, by introducing K_t , without taking into account the plasticity effects due to the high value of strain. The results obtained by the application of this model were still good even if they were based on an approximated consideration of the material behavior. From a detailed analysis of the tested specimen, the spot where the crack initiates was detected moved from the notch root. This distance depended on the value of the notch root radius. The proposed finite element model in this thesis wants to consider the real behavior of the material, focusing on plasticity effects and local values of strain. In order to achieve the proposed aims, the specimens have been modeled by taking into account different levels of hardening in the specimen due to a low cycle multiaxial fatigue test. A good description of this phenomenon has been reported on the hardness maps obtained experimentally after the tests. In order to assign different levels of hardening to the specimen, the cyclic curves of the material obtained with a step-up test have been used. Since the cyclic curves of the material are not enough to describe the gradual variation of hardening, more curves have been obtained. The areas with different

levels of hardening have been shaped as circles to simplify the process of modeling. After the model has been created, a tensile load has been applied, which value was the same of the stresses recorded in the tests. The results have been then analyzed, focusing on the position of maximum strain and the value of stress in that point. The position of maximum strain depended on the value of the notch root radius, confirming that the spot where the crack initiates is moved from the notch tip because of a combination of stress and hardening on the material. Successively, a new $K_{t,n}$, named K_t' , has been calculated as the ratio between the stress obtained in the spot where maximum strain is located and the nominal value of stress. The model has been modified by replacing $K_{t,n}$ with K_t' , to observe if there is some improvement on the results. The new parameter makes the data collapse in a more narrow scatter band giving a better correlation between fatigue life and the strain parameter, compared to the data obtained with the original model. The proposed modeling concept gives also a better interpretation of the real behavior of the material subjected to this type of loading, by taking into account plastic behavior and hardening.

SOMMARIO

Il presente lavoro di tesi ha come obiettivo la realizzazione di un modello agli elementi finiti di un provino intagliato realizzato in acciaio inossidabile del tipo 316L soggetto a fatica multiassiale a basso numero di cicli con carico non proporzionale. I provini modellati e analizzati sono stati precedentemente testati sperimentalmente a fatica in controllo di deformazione, al fine di determinare la relazione tra vita a fatica e deformazione nominale. La relazione tra la durata del provino e la deformazione nominale è stata descritta con un modello che tiene conto sia dell'incrudimento extra dovuto al carico non proporzionale che della gravità di questo carico. Entrambi i parametri vanno a modificare il parametro di deformazione nominale per poi porlo in relazione con la durata a fatica. Originariamente, questo modello era stato applicato per provini lisci con buoni risultati. Successivamente, il modello ha subito una modifica per tenere conto dell'effetto di concentrazione delle tensioni presente in provini intagliati. La modifica prevedeva l'applicazione del $K_{t,n}$ nella formula, senza tenere conto di effetti di plasticità dovuti all'elevato valore di spostamento indotto dai test. I risultati dell'applicazione di questo modello modificato restano comunque buoni ma sono basati su una considerazione del comportamento del materiale approssimativa e non reale. Da un'analisi dettagliata dei provini testati si è visto inoltre come la posizione del sito di innesto della cricca non si colloca all'apice dell'intaglio, ma si trova ad una certa distanza da esso, lungo la superficie dell'intaglio. Questa distanza dipende dal raggio di raccordo dell'intaglio. La modellazione agli elementi finiti proposta in questo lavoro considera il comportamento reale del provino, in particolare gli effetti della plasticità e il parametro locale di spostamento. Per fare ciò si è modellato il provino tenendo conto di differenti livelli di incrudimento che si originano nel componente dopo una prova a fatica multiassiale a basso numero di cicli. Una buona descrizione di

questo fenomeno è ben riportata nelle mappe di durezza ottenute sperimentalmente sui provini testati. Per assegnare al materiale diversi livelli di incrudimento sono state sfruttate le curve cicliche stabilizzate del materiale ottenute da test di tipo step-up. Dato che le curve non sono abbastanza per descrivere il cambiamento graduale di durezza nel provino, è stato necessario ricavare più curve. Le diverse aree incrudite sono state concepite di forma circolare, per semplificare la modellazione. Dopo aver creato il modello, è stato applicato un semplice carico di trazione, il cui valore rispecchia quello dei test a fatica multiassiale. I risultati sono stati poi analizzati concentrandosi sulla posizione del massimo spostamento e il valore di tensione in quel punto. La posizione della deformazione massima dipende dal valore del raggio di raccordo dell'intaglio, confermando i risultati ottenuti nei test. Questo fenomeno è dovuto ad una combinazione di incrudimento e intensità del campo di tensione attorno all'apice. Successivamente, un nuovo $K_{t,n}$, denominato K_t' , è stato calcolato facendo il rapporto tra la tensione ricavata nel punto di massimo spostamento e il valore nominale di tensione. Inserendo nel modello il nuovo parametro, è stato fatto un confronto con i risultati precedenti per osservare la presenza di miglioramenti/peggioramenti. Il nuovo parametro K_t' migliora i risultati stringendo la banda di dispersione, fornendo una miglior correlazione tra la vita a fatica e la deformazione nominale rispetto ai dati ottenuti con il modello originale. La modellazione proposta fornisce inoltre una miglior interpretazione del comportamento reale del materiale soggetto a questo tipo di carico, tenendo conto del comportamento plastico e successivo incrudimento.

INDEX

1. INTRODUCTION	1
2. EXPERIMENTAL PROCEDURE	5
2.1. Specimens material and geometry	5
2.2. Test Conditions	7
2.3. Cyclic curves.....	8
2.4. Hardness tests	9
2.5. Test Results.....	14
3. ITOH-SAKANE MODEL FOR FATIGUE LIFE EVALUATION.....	17
3.1. Model definition	17
3.2. Model for notched specimens.....	18
3.3. Parameters Evaluation	19
3.4. Evaluation with FEA	25
4. SPECIMEN MODELING CONCEPT	27
4.1. Intermediate curves evaluation.....	28
4.2. Example: evaluation of an intermediate curve.	34
4.3. Size and shape of areas	35
5. SPECIMEN FEM ANALYSIS.....	39

5.1. Specimen Geometry.....	39
5.2. Creation of areas	41
5.3. Element type	42
5.4. Material properties.....	45
5.5. Mesh.....	47
5.6. Simulation Conditions	50
6. RESULTS AND DISCUSSION.....	53
6.1. Stress and strain distribution at the notch root	54
6.2. Discussion.....	62
7. CONCLUSIONS.....	65
REFERENCES	67
ACKNOWLEDGEMENTS	69

1. INTRODUCTION

Components and structures in several engineering applications undergo nowadays to multiaxial low cycle fatigue under non proportional loading. Pressure vessels, high temperature exchangers and nuclear vessels of fast breeder reactors are good examples. For the evaluation of fatigue life of components subjected to such critical conditions different approaches have been developed and reported in the recent and past literature. Considering high cycle fatigue life estimation, many studies and researches have been conducted. The developed models were mainly based on local stresses neglecting the small plastic range involved, therefore their applicability was limited to high number of cycles [1–3] . These methods were an extension of static yield criteria to fatigue regime, and they tried to evaluate an equivalent stress in different ways, depending on the selected criteria. Many methods were also developed based on strain range, in order to analyze those situations in which the plastic deformation cannot be anymore neglected, such as in low cycle fatigue regime [4]. However, these approaches still are not suitable in case of non-proportional multiaxial loading. Pioneering works on the life evaluation under non proportional loadings were mainly based on critical plane approaches, such as Fatemi-Socie [5] and Smith-Watson-Topper (SWT) [6]. These models were based on the orientation of crack growth through the definition of a critical crack propagation plane: if crack nucleation is Mode II dominated, fatigue lifetime was estimated by using the torsional Manson-Coffin curve [7]. On the other hand, if the cracking behavior is Mode I governed, fatigue life was estimated by using uniaxial Manson Coffin Curve and the SWT parameter to take into account mean stress effect.

Other authors instead, focused on energetic approaches for the fatigue life assessment under non proportional loadings. Liu [8] and collaborators, for example, proposed a method based on strain energy parameters. The model, considered the elastic and plastic work and presented a good applicability to multiaxial loadings, regardless if they are shear-dominated or tensile-dominated.

Critical plane and energy approaches found good applicability and results in both proportional multiaxial high cycle and low cycle fatigue. However, components might be subjected to non-proportional loading. This condition has a strong influence on fatigue life and hardening behavior of the component: usually life is reduced and an additional hardening is reported compared to proportional loading as reported in several references [7,9,10]. In general, when classical models such as Fatemi-Socie, SWT and Liu are applied for non-proportional loadings, fatigue life tends to be overestimated.

While many studies have been carried out considering non-proportional multiaxial low cycle fatigue for smooth specimens, a limited number of papers have been reported for notched specimens [11,12]. The number of papers available in literature decreases even more when low cycle fatigue under non proportional loading is considered [13,14]. In [15] a study of notched specimens under non proportional multiaxial low cycle fatigue was reported. In that work the number of cycles to crack initiation were found to be significantly influenced by notch radius, leading to an overestimation of number of cycles to crack initiation and failure. In order to take into account this phenomenon, a modified Neuber's rule was proposed. The modified rule gave good results and all the data collapsed within a factor of two scatter band.

Itoh and Sakane proposed a strain based model which takes into account additional hardening and strain path, in order to evaluate a new strain parameter, called non-proportional strain range, to assess failure life. This model has been applied widely for hollow specimens made by different materials, and its

accuracy was verified comparing the results from non-proportional and proportional loadings [16,17]. The results were successfully synthesized in a factor 2 band which suggested a good prediction of fatigue life and an accurate interpretation of the factors involved in the proposed model. In particular, the proposed material dependent parameter was simple to evaluate and the results suggested it was actually representative of the additional hardening occurring in the specimen when undergoes non-proportional loading, considering 2D and 3D strain paths [18,19]. Recently, Itoh *et. al* [20] analyzed notched specimens under proportional and non-proportional low cycle fatigue to evaluate fatigue life. In that work, the Itoh-Sakane model for life evaluation was modified by considering local parameters of strain, in order to take into account the stress concentration factors and particular attention was paid on the evaluation of additional hardening, which depends both on strain path and notch radius.

Non-proportional strain was also evaluated through accurate finite element analysis. Since notched components have stress concentration factor and the analytical rules conventionally used to evaluate local strain tends to overestimate fatigue lives, many FEM models have been proposed in order to evaluate this parameter. Common methods to conduct finite method analysis of multiaxial low cycle fatigue are based on the evaluation of a kinematic hardening rule which tries to describe the hardening process of the material as made in some author's previous works[15,20]. The present work reanalyzes the experimental results reported by Itoh and collaborators [20], proposing a new predictive model taking into account the real strain hardening behavior of the material in the proximity of the notch tip. The new model allows to evaluate the data in a narrow scatter band and provides a sound interpretation of the crack initiation phase. The model is well supported by accurate finite element analysis that consider the real cyclic curves obtained experimentally, in order to give a sound interpretation of the hardening behavior which occurs in the specimen under low

cycle fatigue regime. In particular, the specimen has been divided from numerical viewpoint in different areas, each one with its own level of hardening. Thanks to this technique, faithful plasticity effect has been taken into account. Different notch geometries have been considered ($K_{t,n}=1.5, 2.5, 4.2, 6$) and the local value and position of local strain have been commented and compared with experimental results.

2. EXPERIMENTAL PROCEDURE

This chapter explains how the data of multiaxial fatigue tests have been carried out. These tests have been conducted in order to correlate fatigue life with non-proportional strain [20]. The data have been carried out for notched specimen, in order to modify a model for estimating fatigue life for this kind of components (explained in chapter 3). These results have been used for the FEM modeling, focusing on cyclic curves, hardening process of the material and value of applied stress by the testing machine. Hardness maps of the specimen have been carried out in order to show the mechanical behavior of the material after the tests.

2.1. Specimens material and geometry

Notched specimens are made of type 316L stainless steel (SUS316L) and shows four different stress concentration factors as shown in Fig. 2.1 (a-d). Dimensions are in mm. No heat treatment was applied to the specimen after machining.

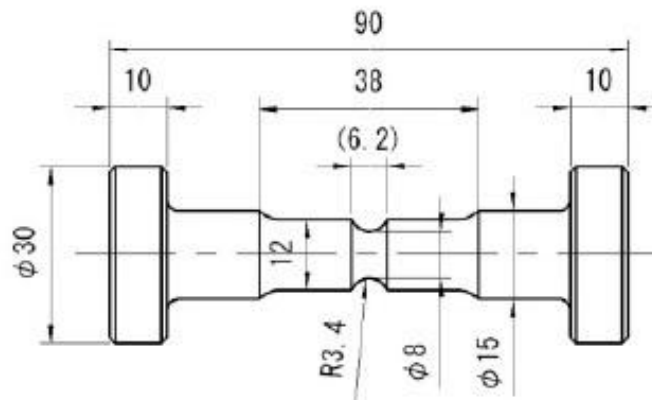


Fig. 2.1 (a) $K_{t,n}$ 1.5 [20]

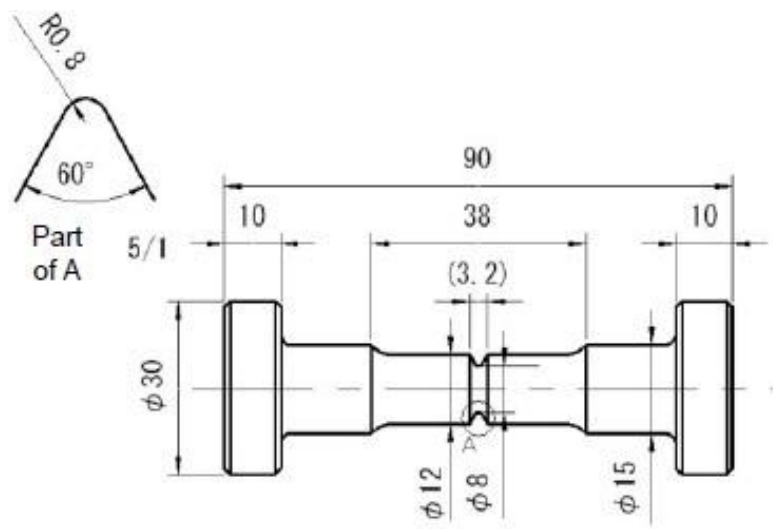


Fig.2.1 (b) $K_{t,n}$ 2.5 [20]

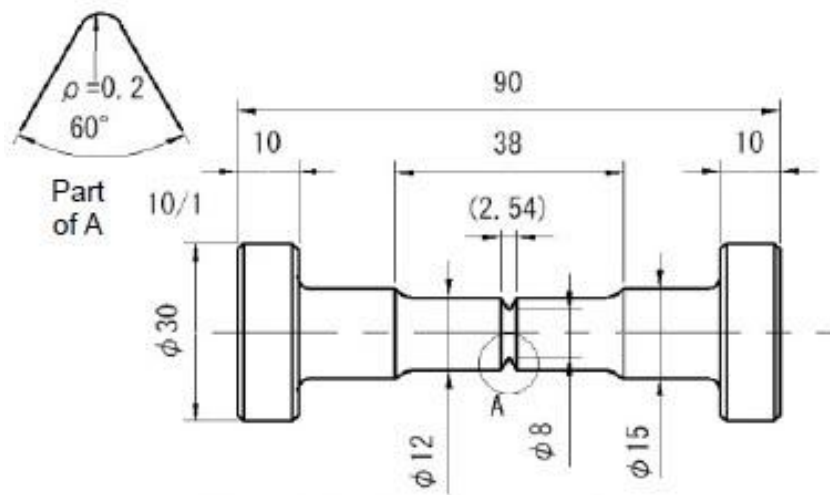


Fig. 2.1 (c) $K_{t,n}$ 4.2 [20]

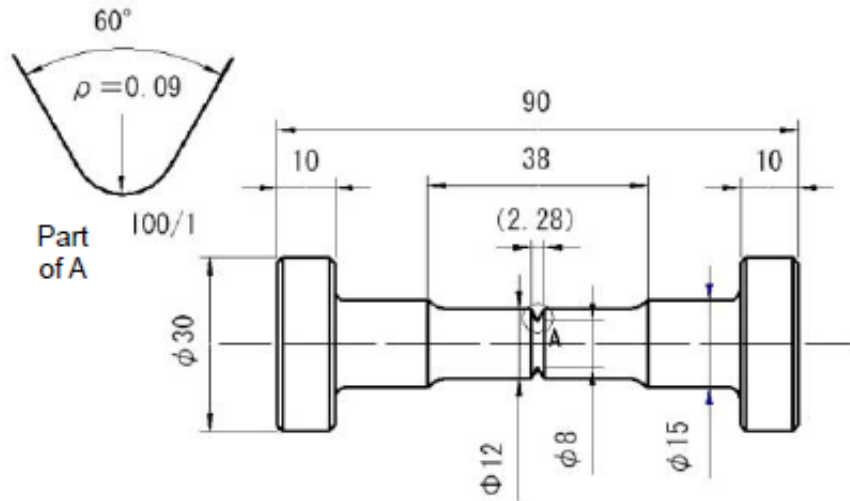


Fig. 2.1 (d) $K_{t,n} 6$ [20]

2.2. Test Conditions

Specimens have been tested with proportional and non-proportional strain paths. Proportional load is represented by push-pull and reverse torsion loading, while non-proportional load by circle strain path, where the equivalent stress and strain values are the same for all the duration of the cycle (Fig. 2.2). The strain paths employed are shown on the $\epsilon\text{-}\gamma/\sqrt{3}$ plot. Since the value of $\Delta\sigma_{eq}$ is the same for each point of the cycle, it is possible to obtain a cyclic curve plotted in a $\Delta\sigma_{eq}/2$ - $\Delta\epsilon_{eq}/2$ graphic.

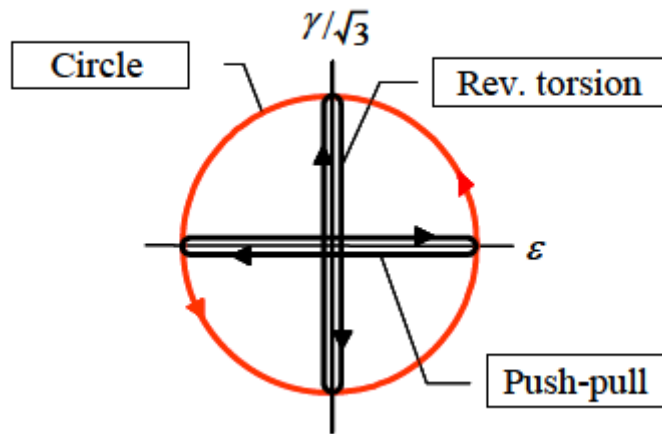


Fig. 2.2 Strain Paths employed in experimental procedure. [20]

Tests were made by applying an equivalent strain range (Von Mises) $\Delta\epsilon_{eq}=0.7\%$. Gage length for measuring axial and shear displacement by an extensometer was 7mm for all type of specimens. For these tests the number of cycles to failure was defined as the number of cycles at which stress amplitude becomes 3/4 of the maximum value.

2.3. Cyclic curves

Cyclic curves were carried out from a step up test where strain range was increased by 0.1% every 10 cycles (Fig. 2.3). This simulation used only push-pull and circle cyclic curves.

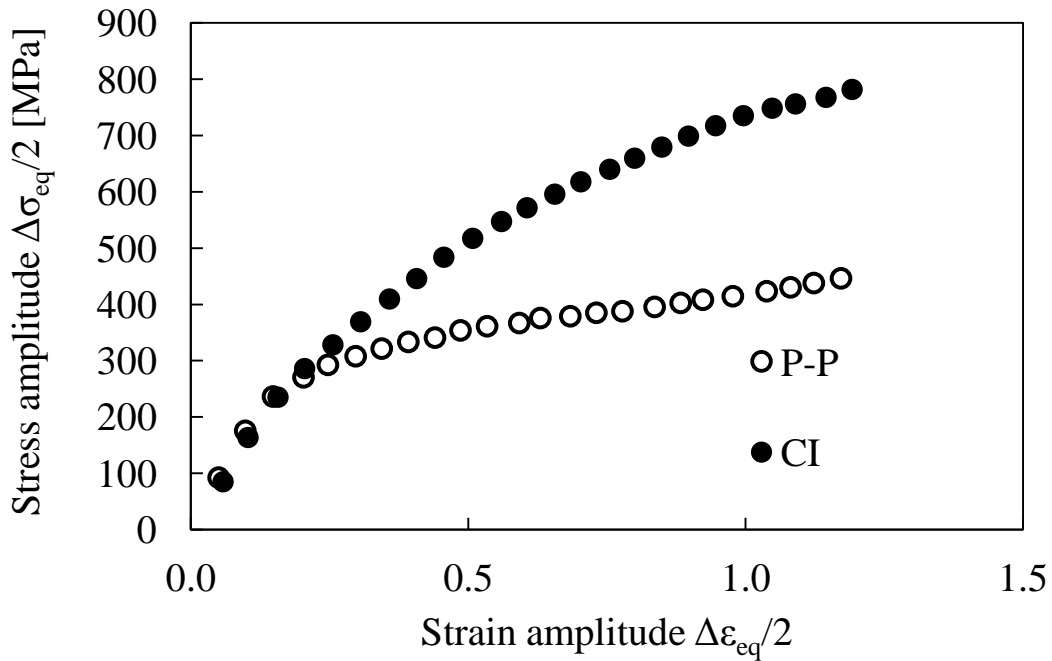


Fig. 2.3 Cyclic Curves for Circle (CI) and Push-Pull (P-P) tests.[20]

These cyclic curves are representative for SUS316L and they don't depend on stress concentration factors. Therefore, they have been used to model all the geometries ($K_{t,n}$ 1.5, 2.5, 4.2 and 6).

2.4. Hardness tests

Value of hardness has been carried out for all the specimens and strain paths, by interrupting the test at $0.3N_f$ and sawing the specimen along the axis for the evaluation of hardness on 5 directions. See Fig. 2.4, 2.5.

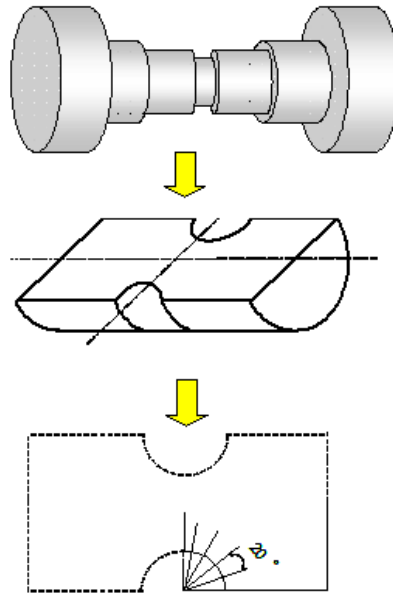


Fig. 2.4 Cut direction

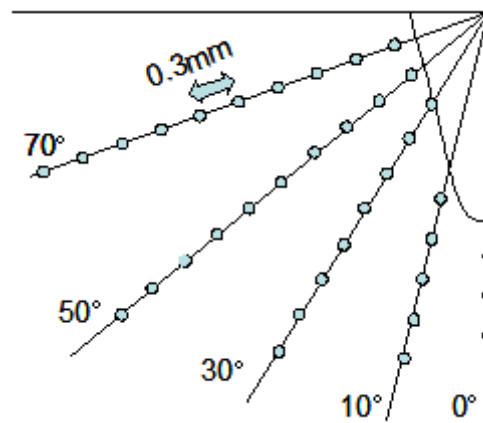


Fig. 2.5 Spots for HV hardness evaluation

In order to understand how notch radius and non-proportionality have influence on the final value of hardening, graphics of hardness are shown in Fig. 2.6 (a-b) and they represent this parameter on the 0 degree direction.

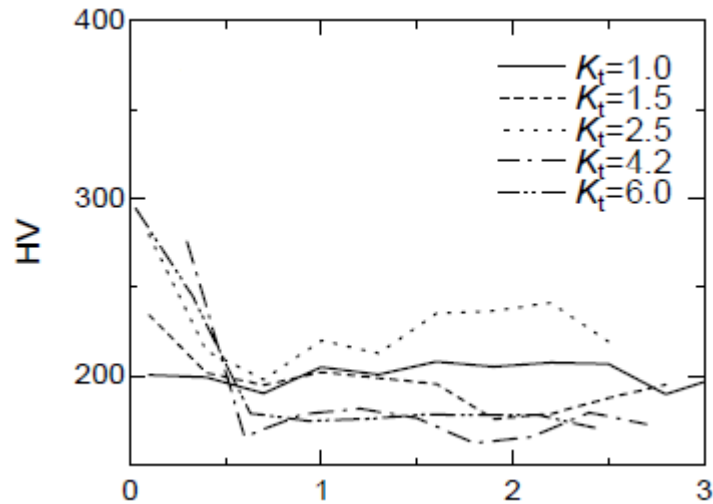


Fig. 2.6 (a) Hardness for Push-Pull tests along 0 degrees direction [20]

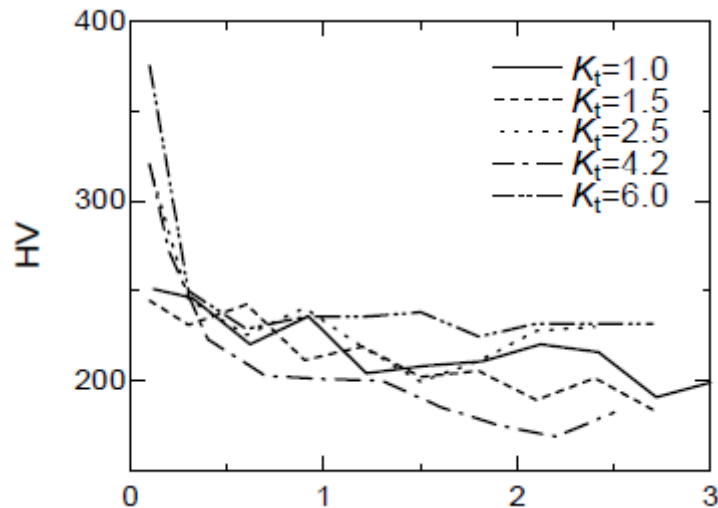


Fig. 2.6 (b) Hardness for Circle tests along 0 degrees direction [20]

In push-pull, obvious hardening occurs for notched specimens near the notch root.

The maximum value of hardness in $K_{t,n}=2.5-6$ shows almost the same level. $K_{t,n}=1.5$ shows the intermediate level between those of $K_{t,n}=1$ and $K_{t,n}=1.5-6$. The results show that the degree of cyclic hardening increment in the Push-Pull test due to notch has a limit around HV200 for 316L. The cyclic hardening increment near the notch root in the circle test can also be seen and the maximum value of hardness is much larger than in Push-Pull. This result

suggests that the additional hardening exists due to non-proportional loading. Moreover, a small cyclic hardening can be seen in rev. torsion. In summarizing above results, the additional hardening which occurs in notched specimens under non-proportional loading depends on both strain path and $K_{t,n}$, which may have some effects on lives. From these tests, hardness maps can be obtained by the values obtained in the spots shown in Fig. 2.5. These maps are not accurate because they are based on values obtained in a finite number of spots but they are useful to give a general vision of the hardness into the specimens, after they undergo different types of strain paths. In Fig. 2.7, a limited cases of hardness maps are reported ($K_{t,n}$ 4.2 and 6 for push-pull and circle path). These maps have been used to make a comparison with the FEM model created for this work.

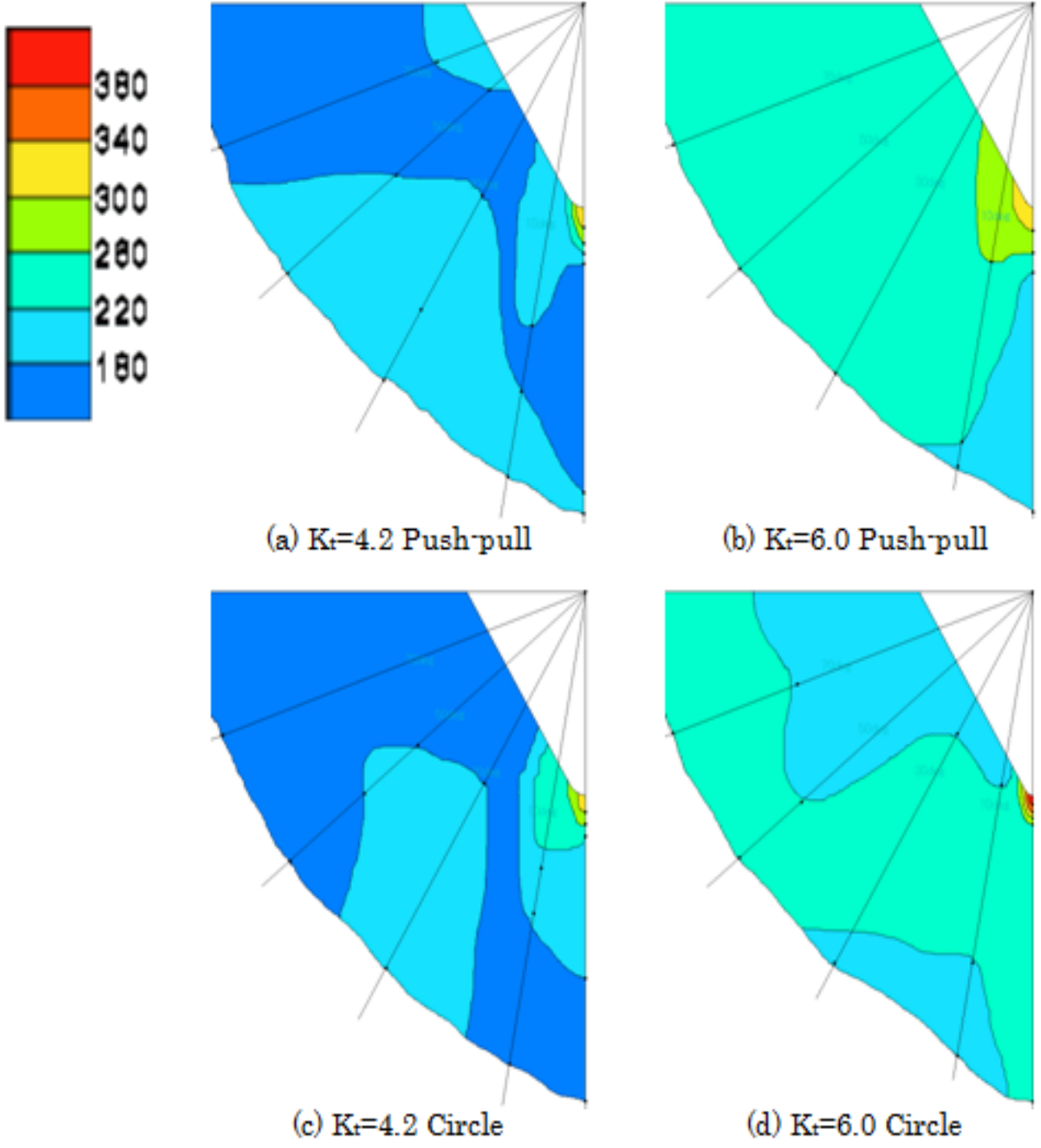


Fig. 2.7 Example of hardness maps obtained by hardness tests

2.5. Test Results

The results summarized in Table 1 shows the number of cycles to failure for all the specimen subjected to all strain paths.

Tab.1 Experimental N_f and applied $\Delta\sigma$. [20]

Strain Path	$K_{t,n}$	$\Delta\sigma$ at $1/2 N_f$ (MPa)	$\Delta\tau$ at $1/2 N_f$ (MPa)	N_f
Push-Pull	1	680	-	6909
	1.5	800	-	2237
	2.5	800	-	871
	4.2	810	-	571
	6	830	-	418
Circle	1	780	1050	2082
	1.5	850	1030	2248
	2.5	880	1080	475
	4.2	900	1140	212
	6	850	930	156
Reverse Torsion	1	-	600	Run Out
	1.5	-	720	54809
	2.5	-	910	4806
	4.2	-	890	3094
	6	-	850	2243

As expected, fatigue life decreases the higher is stress concentration factor. Furthermore, fatigue life is lower for non-proportional loading compared to proportional loading for same $K_{t,n}$ because of additional hardening and non-proportional effect.

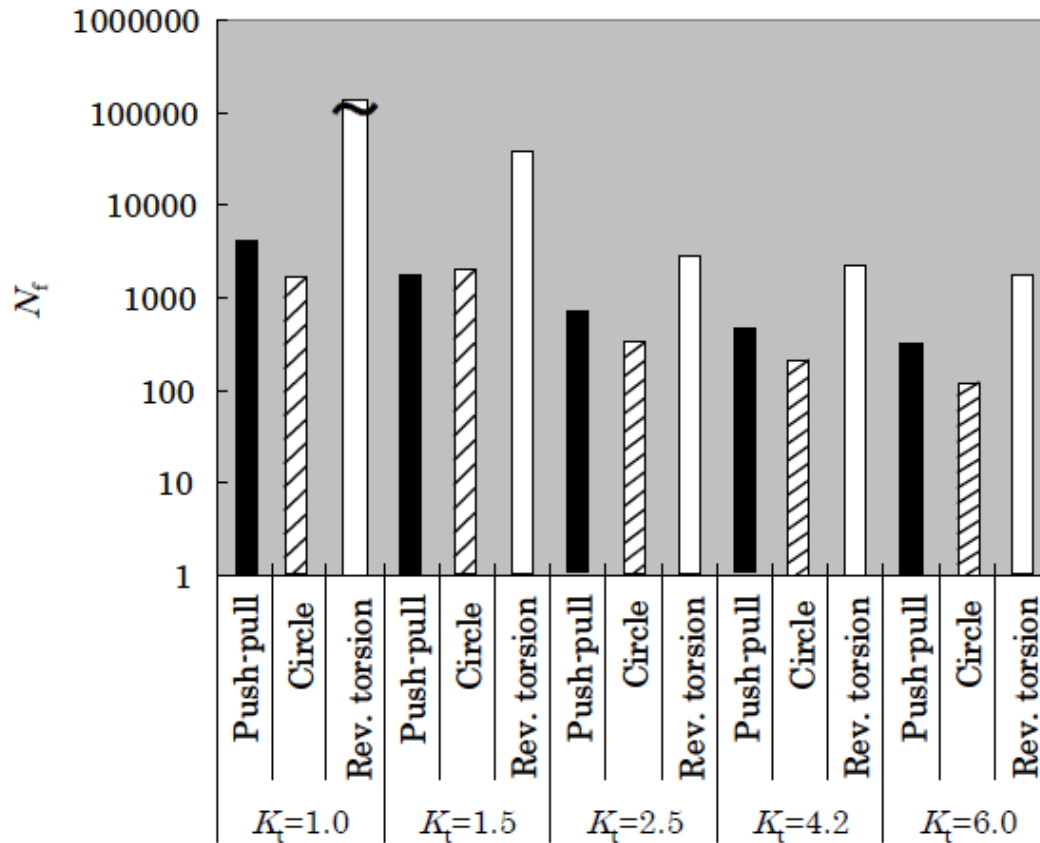


Fig. 2.8 Fatigue life for different specimens and strain paths [20]

Fig. 2.8 shows the results in terms of fatigue life.

In push-pull, N_f decreases with increasing $K_{t,n}$. In $K_{t,n}$ 6, N_f becomes approximately 6% of that in $K_{t,n}=1$. However, in circle, N_f at $K_{t,n}=1.5$ is slightly higher than the one of smooth specimen but N_f decreases with increasing $K_{t,n}$ in the range $K_{t,n}=2.5-6$. The longer life shown in $K_{t,n}=1.5$ of circle may be the result of the additional hardening which reduces the strain amplitude at notch part. Stainless steels are known as materials which show large additional hardening due to non-proportional cyclic loading, so the fatigue life in $K_{t,n}=1.5$ was influenced by the additional hardening dominantly rather than the stress and strain concentration at the notch root when $K_{t,n}$ is small. The failure life for SUS316L was affected largely by both the notch and the strain.

By analyzing in detail the tested specimen, the position of the crack initiation spot was detected moved from the notch tip as shown in Fig (2.9).

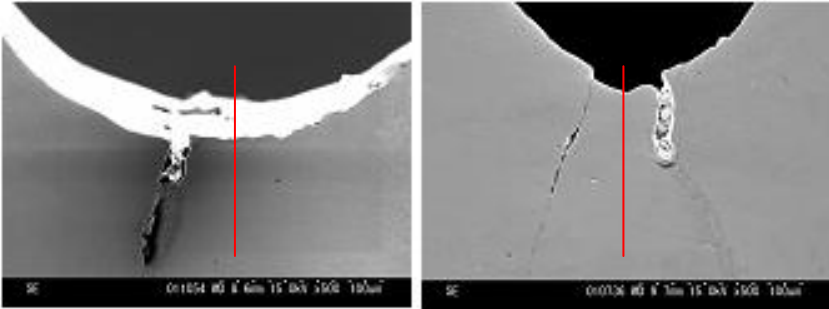


Fig 2.9 Fractures on $K_{t,n}$ 4.2 and 6

This behavior was probably due to a combination of stress and hardening around the notch tip, suggesting that the stress concentration factor $K_{t,n}$ commonly defined might be incorrect to consider for the fatigue life estimation. If the crack initiates in a point moved from the tip, local parameter of stress and strain in that point must be considered for a more accurate estimation.

3. ITOH-SAKANE MODEL FOR FATIGUE LIFE EVALUATION

This chapter shows and discusses the model used to correlate fatigue life and a strain parameter. The model has been used widely for smooth specimens, giving good results. It was also used in a lower amount of cases for notched specimens, one of which is the experimental work discussed in chapter 2. This model is useful to evaluate fatigue life, as it takes into account some phenomena which distinguish non-proportional loading: non-proportional loading intensity and additional hardening.

3.1. Model definition

This model was originally introduced for smooth specimen to assess failure life for different materials subjected to proportional and non-proportional loadings [18]. The proposed model considers two factors for evaluating failure life: non proportional factor f_{NP} , which express the intensity of non-proportional loading and material constant α , which is related to the material additional hardening due to non-proportional loading. Given these factors it is possible to evaluate a strain parameter starting from the experimental nominal strain rate:

$$\Delta\varepsilon_{NP} = (1 + \alpha f_{NP})\Delta\varepsilon_1 \quad (1)$$

In the case of SUS316L, $\alpha=0.9$. Non proportional factor, f_{NP} , takes the value of 1 for circle load path and 0 for push-pull.

This model can be applied for smooth specimens since $\Delta\varepsilon_1$ is the nominal and maximum strain range (there is not stress concentration factor).

3.2. Model for notched specimens

Since many components have a complicated shape, stress concentration may occur. In this case $\Delta\varepsilon_1$ does not correspond anymore to maximum strain because of geometrical discontinuities. It's consequently necessary to evaluate $\Delta\varepsilon_{NP}$ starting from local strain. The main problem on applying this model on notched specimens, as in this case, is the difficulty on the evaluation of local maximum strain since the material is not behaving elastically. Itoh *et al.* tried to apply the relationship between $\Delta\varepsilon_{NP}$ and N_f to notched specimens, by evaluating the local stress by the application of $K_{t,n}$, assuming that local strain is positioned at the tip.

$$K_{t,n}\Delta\varepsilon_{NP} = K_{t,n}(1 + \alpha f_{NP})\Delta\varepsilon_1 \quad (2)$$

Results of the application of this model are summarized in Fig. 3.1. The scatter band represent datas for hollow smooth specimen obtained in an author's previous work [18]: non-proportional strain range can be well correlated with N_f even for notched specimens.

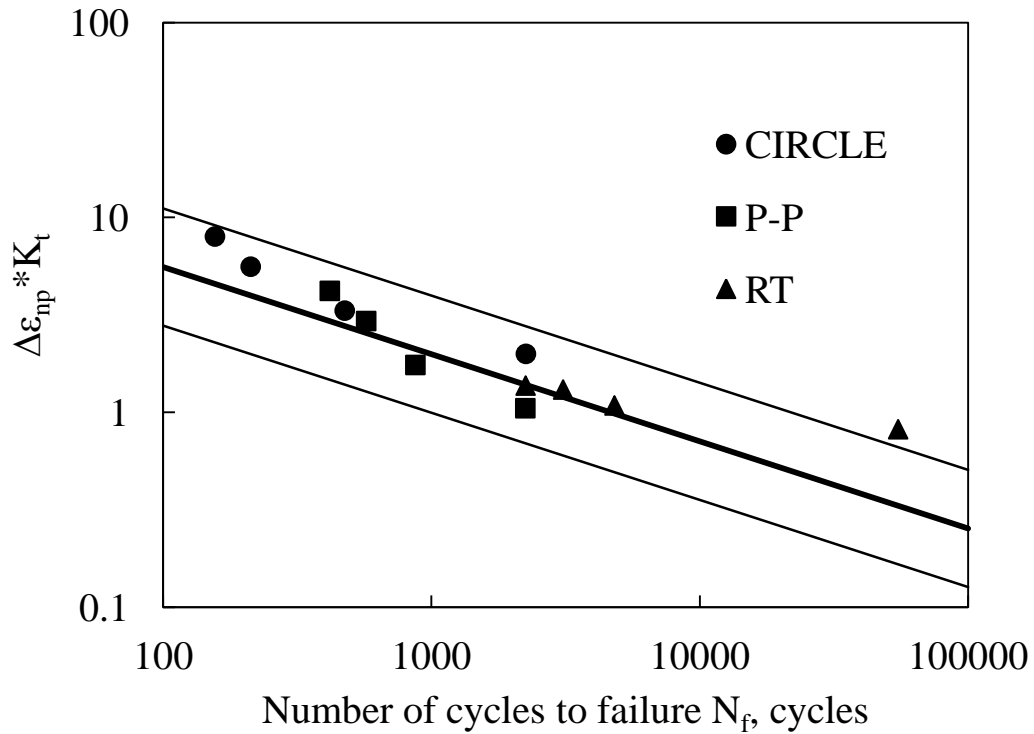


Fig.3.1 Correlation between $\Delta \epsilon_{np}$ and N_f for push-pull (P-P), reverse torsion (RT) and circle load paths.

However, since $K_{t,n}$ is evaluated for stresses in elastic field, it might be theoretically incorrect to apply this factor, since plastic deformation occurs in components which undergo low cycle fatigue. Neuber's rule can be applied to evaluate local strain even if the analytical application of this rule tends to overestimate fatigue life [15].

3.3. Parameters Evaluation

1) f_{NP}

Fig. 3.2 illustrates three principal vectors $S_1(t)$, applied to a small cube in material at time t in xyz -coordinates (spatial coordinates), where "S" is the symbol denoting either stress " σ " or strain " ϵ ". Thus, $S_1(t)$ are the principal stress

vectors for the case of stress and are the principal strain vectors for the case of strain. The maximum principal vector, $S_I(t)$, is defined as $S_i(t)$ whose absolute value takes maximum one, $S_I(t)=S_1(t)$ when $S_1(t)$ takes maximum magnitude among $S_i(t)$. The maximum principal value, $S_I(t)$, defined as the maximum absolute value of $S_i(t)$.

$$S_I = |S_I(t)| = \text{Max}[|S_1(t)|, |S_2(t)|, |S_3(t)|] \quad (3)$$

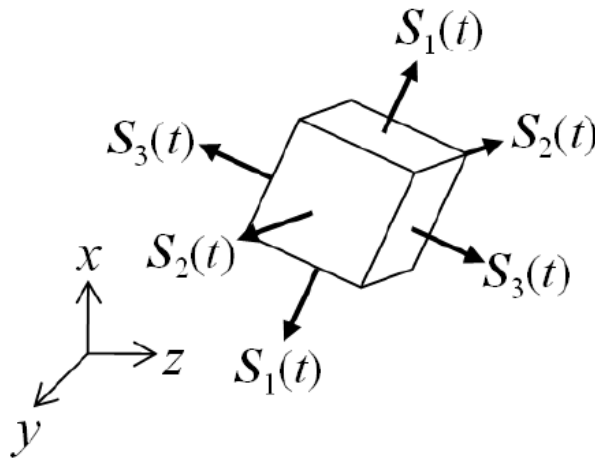


Fig 3.2 [19]

The "Max" denotes taking the larger value from the three in the bracket. The maximum value of $S_I(t)$ during a cycle is defined as the maximum principal value, $S_{I\text{Max}}$, at $t=t_0$ as follows

$$S_I = |S_I(t_0)| = \text{Max}[|S_1(t_0)|, |S_2(t_0)|, |S_3(t_0)|] \quad (4)$$

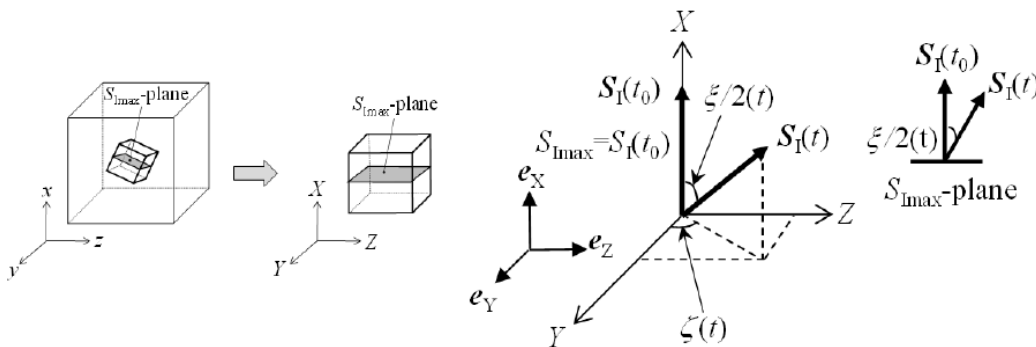


Fig. 3.3[19]

Fig. 3.3 illustrates two angles, $\xi(t)/2$ and $\zeta(t)$, to express the rotation or direction change of the maximum principal vector, $S_I(t)$, in the new coordinate system of XYZ, where XYZ-coordinates are the material coordinates taking X-axis in the direction of $S_I(t_0)$ with the other two axis in arbitrary directions. The two angles of $\xi(t)/2$ and $\zeta(t)$ are given by:

$$\frac{\xi(t)}{2} = \cos^{-1} \left(\frac{S_i(t_0) \cdot S_i(t)}{|S_i(t_0)| |S_i(t)|} \right) \quad (5)$$

$$\zeta(t) = \tan^{-1} \left(\frac{S_i(t) \cdot e_Z}{S_i(t) \cdot e_Y} \right) \quad (6)$$

The dots in equations (5) and (6) denote the inner product and e_Y and e_Z are unit vectors in Y and Z directions, respectively. $S_i(t)$ are the principal vectors of stress or strain used in eq(4) .

The rotation angle of $\xi(t)/2$ expresses the angle between the $S_I(t_0)$ and $S_I(t)$ directions and the deviation angle of $\zeta(t)$ is the angle of $S_I(t)$ direction from the Y-axis in the X-plane.

Fig. 3.4 shows the trajectory of $S_I(t)$ in 3D polar figure for a cycle where the radius is taken as the value of $S_I(t)$, and the angles of $\xi(t)$ and $\zeta(t)$ are the angles shown in the figure. A new coordinate system is used in Fig. 3.4 with the three axes of S_I^1, S_I^2 and S_I^3 , where S_I^1 -axis directs to the direction of $S_I(t_0)$. The rotation angle of $\xi(t)$ has double magnitude compared with that in the specimen shown in Fig. 3.3 considering the consistency of the angle between the polar figure and the physical plane presentation. The principal range, ΔS_I , is determined as the maximum projection length of $S_I(t)$ on the S_I^1 -axis. The mean value, $S_{I\text{mean}}$, is given as the center of the range. ΔS_I and $S_{I\text{mean}}$ are equated as,

$$\Delta S_I = \text{Max}[S_{I\text{max}} - \cos\xi(t)S_I(t)] = S_{I\text{max}} - S_{I\text{min}} \quad (7)$$

$$S_{I\text{mean}} = \frac{1}{2}(S_{I\text{max}} + S_{I\text{min}}) \quad (8)$$

S_{Imin} is the $S_I(t)$ to maximize the value of the bracket. The sign of S_{Imin} in the figure is set to be positive if it does not cross the S_I^2 - S_I^3 plane and the sign negative if it crosses the plane.

The advantage of the definitions of the maximum principal range and mean value mentioned above is that the two are determinable unequivocally for any loading case in 3D stress and strain space. The range and mean value are consistent used in simple loading cases which are discussed in the case studies in the followings. $S_I(t)$ can be replaced by equivalent values of stress or strains, such as the von Mises and the Tresca, in case of necessity from user's requirement.

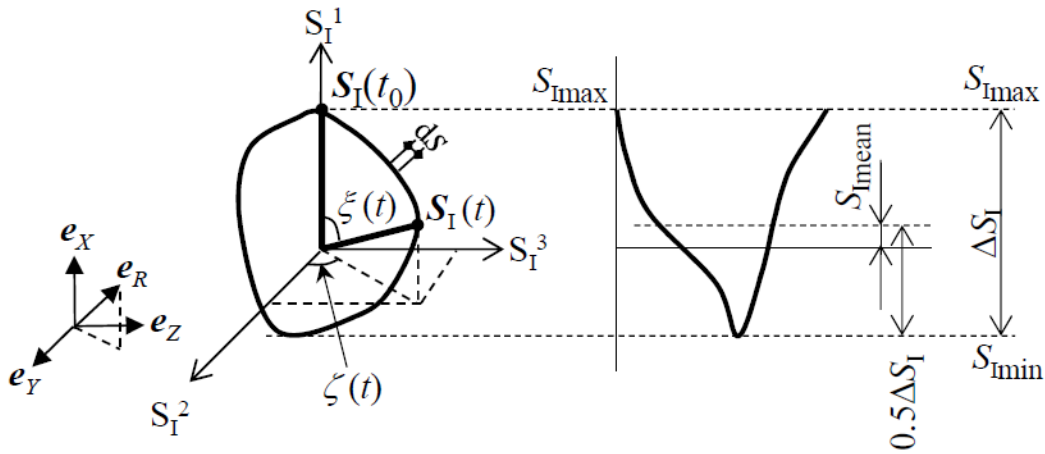


Fig 3.4 [19]

f_{NP} can be defined in different ways.

The first is:

$$f_{NP} = \frac{b}{T \varepsilon_{I MAX}} \int_0^T (|\sin(\xi(t))| |\varepsilon_I(t)|) dt \quad (9)$$

f_{NP} is calculated by measuring the rotation of the maximum principal strain direction and the integration the strain amplitude after the rotation. Therefore, f_{NP} evaluates comprehensively the severity of non-proportional cyclic loading based on the amplitude of strain and the direction change of principal strain.

Another method can be used to evaluate f_{NP} even for 3D stress and strain space defined in previous paragraph, which is expressed as:

$$f'_{NP} = \frac{\pi}{2S_{IMAX}L_{PATH}} \int_C |e_1 \times e_R| S_1(t) ds \quad (10)$$

where e_r is a unit vector directing to $S_1(t)$, ds the infinitesimal trajectory of the loading path shown in Fig. 3.4. L_{PATH} is the whole loading path length during a cycle and "x" denotes vector product. The scalars, S_{Imax} and L_{PATH} , before the integration in eq 10 is set to make

f'_{NP} unity in the circular loading in 3D polar figure. Integrating the product of amplitude and principal direction change of stress and strain by path length in eq 10 is more suitable for evaluation of fatigue damage rather than the integration by time.

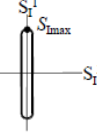


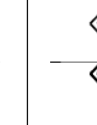

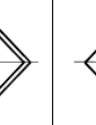
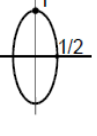
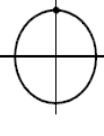
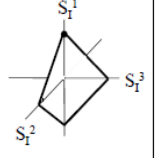

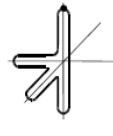

Type	1	2	3	4	5	6
Loading path						
f_{NP}	0	0.39	0.10	0.20	0.79	0.79
f'_{NP}	0	0.49	0.12	0.24	0.71	0.71
Type	7	8	9	10	11	12
Loading path						
f_{NP}	0.53	1.06	-	-	-	-
f'_{NP}	0.5	1	0.71	0.98	0.49	1.78

Fig 3.5 Comparing f_{NP} and f'_{NP} under several loadings. [19]

In this case, f_{NP} for circle has been set as 1.

2) α

In multiaxial LCF of austenite stainless steels, failure life decreases drastically under non-proportional loading accompanying a large additional hardening. This reduction has close relation with the strain path and material. Since the

additional hardening depends on the material, many results have been carried out for different materials [18]. It has been demonstrated how the crystal structure has influence on the MALCF life evaluation since the hardening process is different. As previously said, a good estimation of a strain parameter has been proposed by Itoh *et al.* [17] in order to take into account non-proportional loading and the additional hardening.

$$\Delta\varepsilon_{NP} = (1 + \alpha f_{NP})\Delta\varepsilon_1 \quad (11)$$

The factor α depends on the material and, in particular, on how it hardens under multiaxial loadings effect. The higher is the number, the higher is the difference between the cyclic curves obtained with a strain controlled uniaxial fatigue test and a multiaxial fatigue test, with the application of the same equivalent strain range (Fig 3.6).

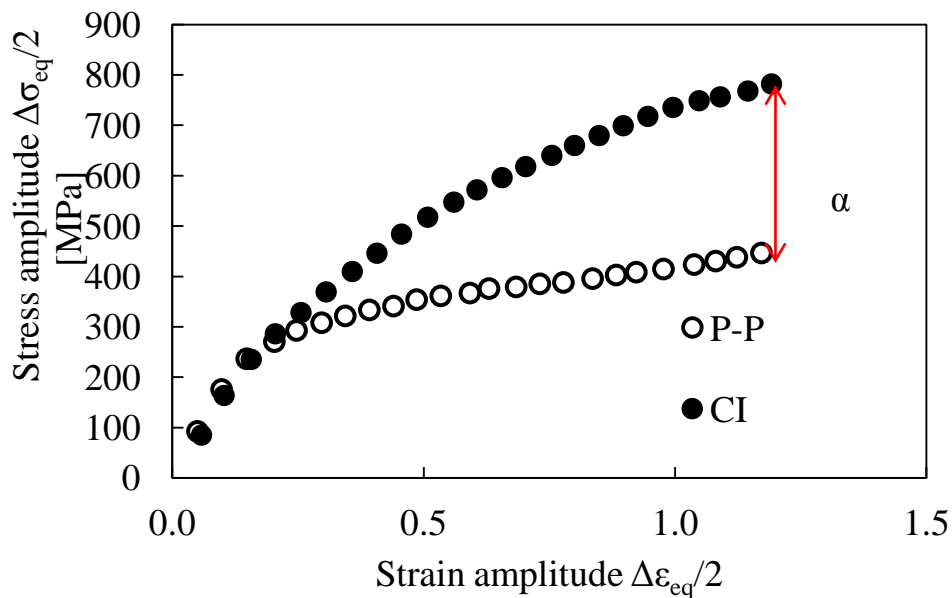


Fig. 3.6 α parameter describes the difference between proportional (P-P) and non proportional (CI) cyclic curve due to additional hardening.

This factor can be obtained in two ways:

- 1) σ ratio method

This method has been used to obtain the material constant in this work. At first, is necessary to obtain the cyclic curves of push-pull and circle loading paths (Fig. 3.7).

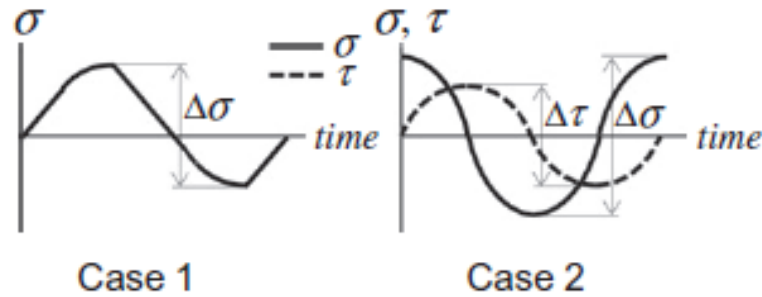


Fig. 3.7 Load cycles

After the specimen has been tested, values of maximum stress range during the cycle must be taken (Table 1, Pag. 15).

Since values are many due to the different values of $K_{t,n}$, medium value of $\alpha=0.9$ has been taken .

$$\alpha = \frac{\Delta\sigma_{eq/2_{Push-Pull}}}{\Delta\sigma_{eq/2_{Circle}}} \quad (12)$$

2) N_f method

Another method to define α is as N_f in Circular loading becomes the failure life equivalent to N_f in Push-Pull at the same $\Delta\epsilon_1$.

3.4. Evaluation with FEA

Another solution is to make a finite method analysis in order to evaluate local parameters. In the work from which the experimental data have been taken [20], an FEA has been conducted as follows: a kinematic hardening rule for the

material has been assigned, trying to predict how the material would have hardened. A cyclic load path (proportional and non-proportional) was applied as a simulation of experimental procedure [15,20]. This type of concept in simulation has been changed in this thesis by modeling the specimen as already hardened and applying an axial loading instead of giving an hardening rule and test the specimen with a cyclic loading.

4. SPECIMEN MODELING CONCEPT

As already stated in the introduction and in the previous section, the application of Sakane-Itoh model relies on the knowledge of local parameters that can be evaluated through different ways: on the basis of linear elastic behavior neglecting the plastic contribution; through a finite element analysis in order to take into account the plastic effects and hardening occurring at the notch tip. From Fig. 2.7 (Pag. 13), it emerges that the hardening occurred around the notch tip is not uniform, but different zones with different levels of hardening can be observed. In order to faithfully replicate this behavior in numerical simulations, a particular technique has been employed: the notch tip has been divided in different hardening areas, and a cyclic curve has been assigned to each area. Even if a simplification, circular areas have been modeled. From experimental tests, push-pull and circle test cyclic curve have been evaluated. They represent the minimum and maximum hardness, respectively. For this reason, the push-pull cyclic curve has been assigned to the material close to the axis of symmetry far from the notch tip, while the circle test cyclic curve to the outer surface of the notch tip. The choice is supported by the hardness maps obtained experimentally, that show a gradually decrement of the hardness moving away from the notch tip. The same hypothesis can be drawn by simple considerations based on the shear stress: as shown in Fig. 4.1 , shear stress assumes maximum value at the outer surface that corresponds to a circle strain paths, at the axis, instead, the shear stress becomes zero, and a push-pull load condition can be assumed.

Later, through best fitting and extrapolation procedures, intermediate cyclic curves to be assigned to the intermediate circular areas have been estimated and modeled following the variation of shear stress in percentage values. In detail, as

limit conditions, circle curve was related to 100% of shear stress while Push-Pull to 0%. The procedures followed for the determination of the intermediate cyclic curves is presented exhaustively in the next section.

Thanks to this modeling technique, the cyclic hardening behavior has been intrinsically taken into account, and a static axial loading corresponding to the maximum axial nominal stress range recorded in experimental tests (see Table 1, Pag. 14) has been applied. As a result, values and positions of local strain and stresses have been obtained.

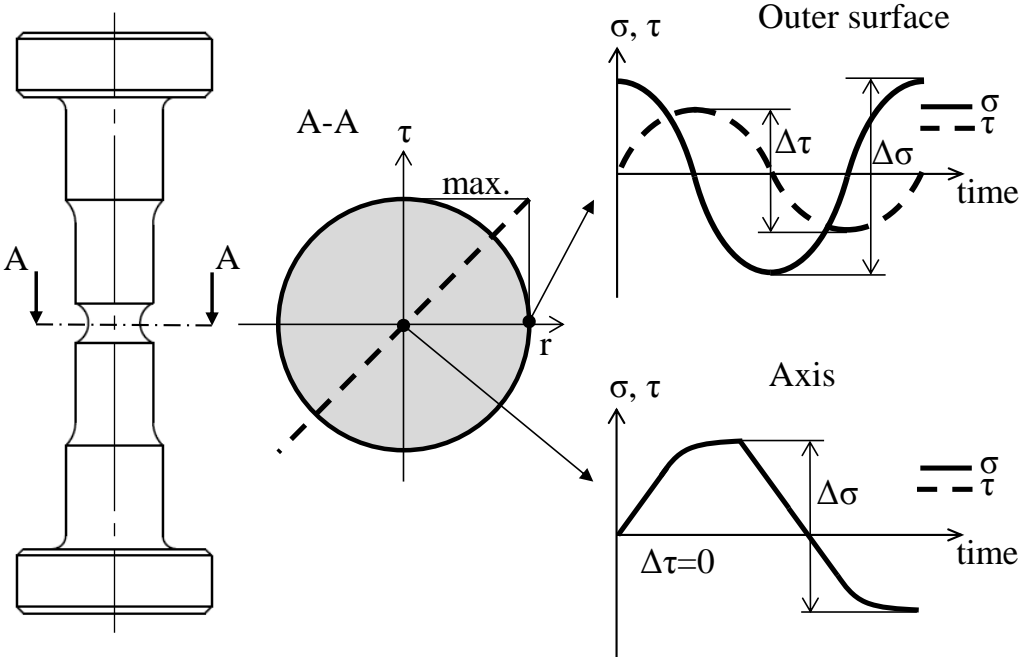


Fig. 4.1 Effectiveness of Circle load at the axis and outer surface: shear stress is maximum at the outer surface and null at the axis.

4.1. Intermediate curves evaluation

First of all, it has been necessary to obtain the equations which describe the cyclic curves already obtained experimentally in order to modify the parameters and obtain the other curves. The following material power law constitutive equation has been employed to describe the cyclic non-linear relationship between the stress and plastic strain:

$$\Delta\sigma = K'\Delta\varepsilon^{n'} \quad (13)$$

The parameters K' and n' , have been obtained through best fitting procedures of the plastic trend of P-P and CI curves shown in Fig 4.2, 4.3 respectively:

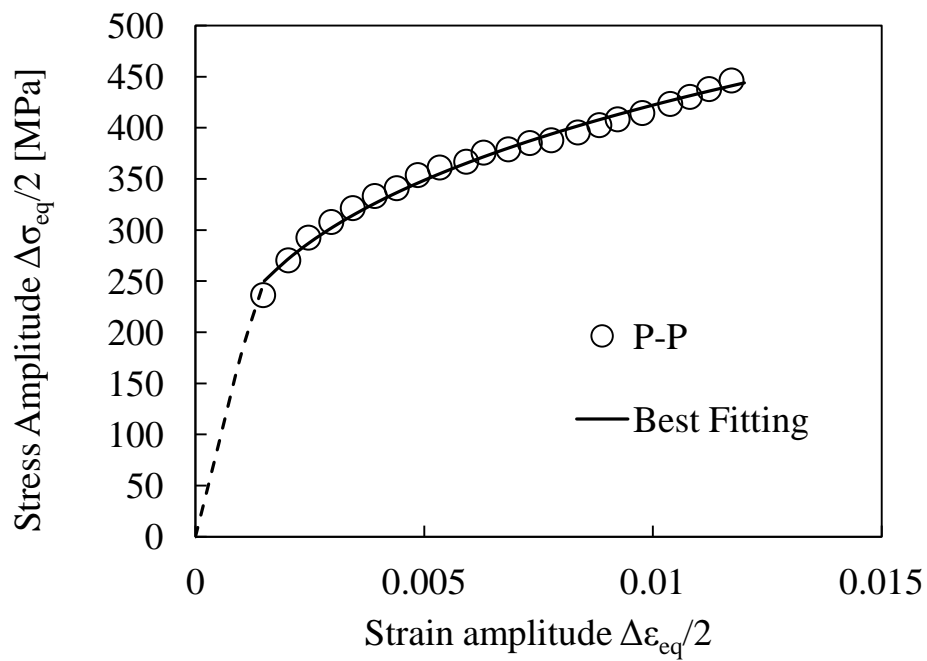


Fig. 4.2 Best fitting of experimental Push-Pull cyclic curve

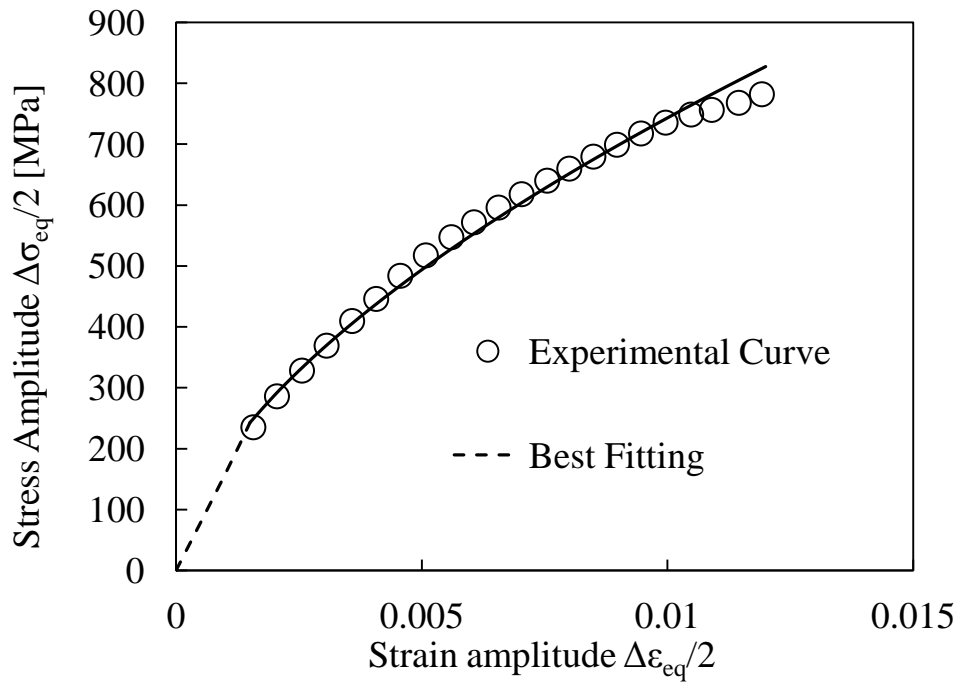


Fig. 4.3 Best fitting of experimental Circle cyclic curve

The equations of the cyclic curves have been obtained:

$$\Delta\sigma = 1502\Delta\epsilon^{0.2756} \quad (14)$$

$$\Delta\sigma = 11210\Delta\epsilon^{0.5893} \quad (15)$$

After the cyclic curves have been described with a constitutive material equation, it could be possible to obtain the intermediate curves by modifying K' and n' parameters. K' and n' for intermediate curves have values in a range of 1502-11210 and 0.2756-0.5893 respectively. Since cyclic curves are the same for each $K'_{t,n}$, the shear stress percentage has been taken into account. Circle curve represents the 100% of shear stress while Push-pull curve represents 0% of shear stress. A curve which stays between those curves represents 50% of shear stress.

Since it was not sure that K' and n' changed with a linear behavior between push-pull and circle (it's not sure that the curve in the middle has K' and n' which are half of K' and n' of circle curve) it was necessary to evaluate a function describing the variation of these two parameters, which required in input the shear stress percentage. Giving these functions, it has been easy to evaluate a single curve's function which stayed between circle and push pull, by evaluating parameters which depended on shear stress percentage. To evaluate K' and n' variation, only few curves have been obtained by imposing a certain percentage of stress for all the values of strain given by experimental curves, in order to obtain a curve corresponding to a certain percentage of shear stress (Fig. 4.4). After the points have been plotted, another regression of these few curves with the same constitutive equation has been done in order to obtain K' and n' for these curves with the same process used for circle and push-pull.

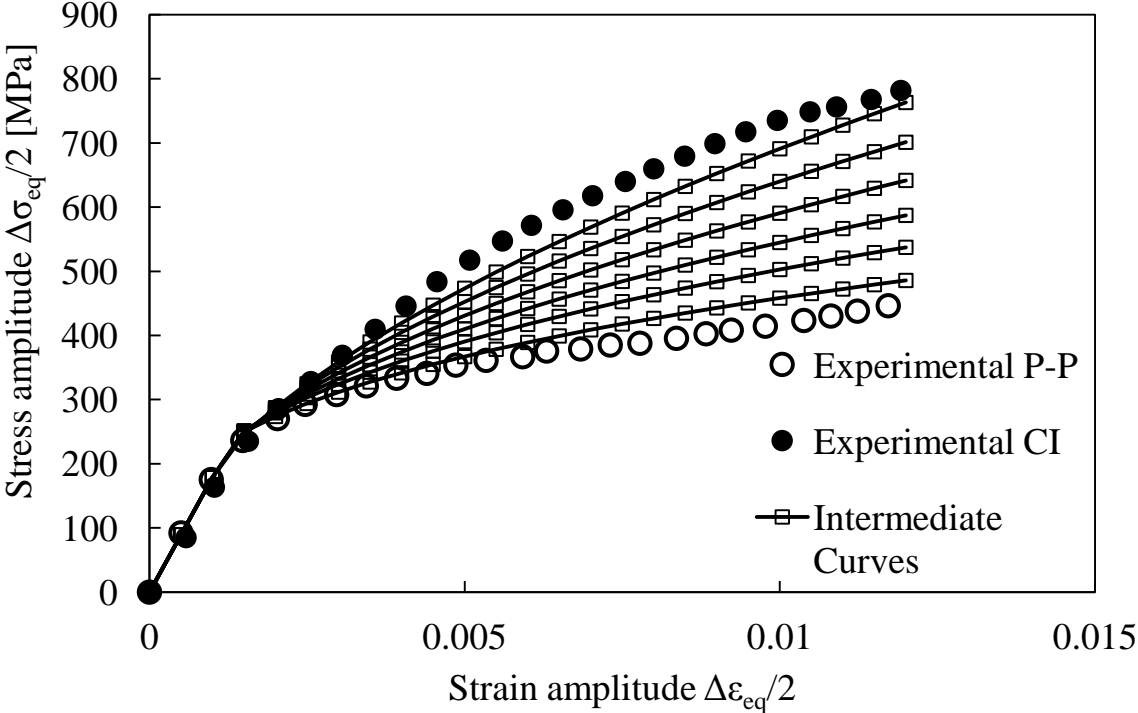


Fig 4.4. Intermediate Curves for the evaluation of K' and n' variation

After those parameters have been obtained (only for 20, 40, 60 and 80% of shear stress) a graphic has been plotted for K' and n' as can be seen in Fig. 4.5, 4.6.

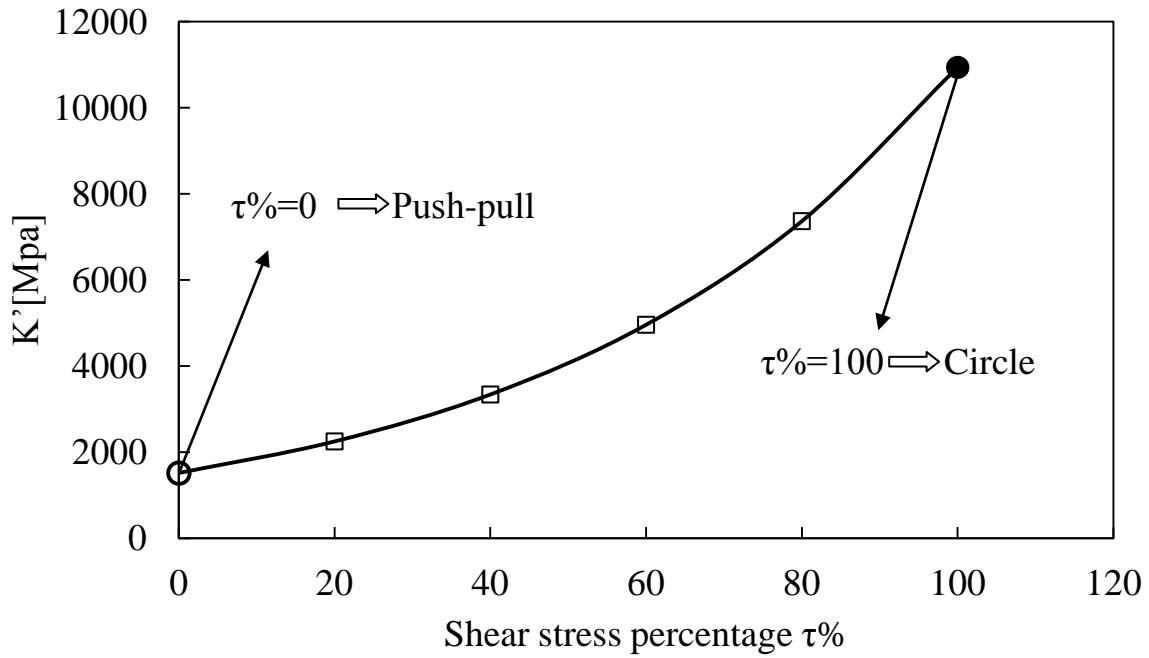


Fig. 4.5 K' variation between Push-Pull and Circle curves.

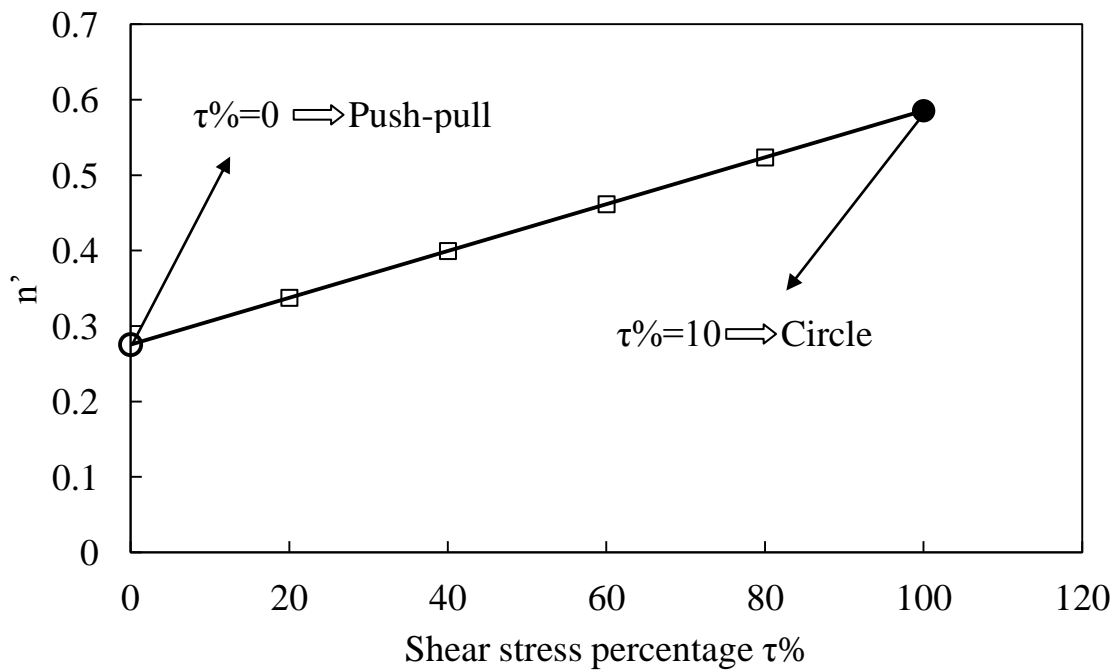


Fig. 4.6 n' variation between Push-Pull and Circle curves.

The dots represent the curves that have been calculated by imposing a shear stress percentage.

By joining those points and fitting the line, two equations have been obtained:

$$K' = 1510e^{0.0198(\tau\%)} \quad (16)$$

$$n' = 0.0031(\tau\%) + 0.2754 \quad (17)$$

K' has an exponential behavior while n' has a linear behavior.

It could be possible to obtain an endless number of curves between push-pull and circle, depending on the desired resolution of the model. Figure 4.7 depicts an example of the cyclic curves obtained varying hardening parameters according to Eq. (16) and (17).

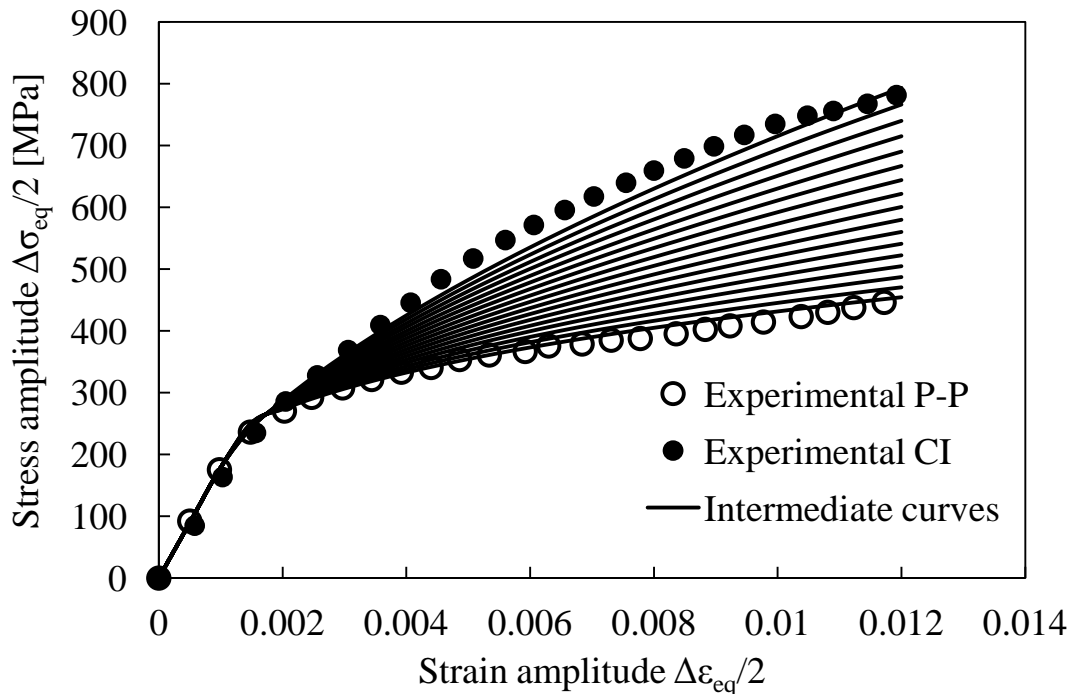


Fig. 4.7 Example of curves obtainable with the equations of K' and n' .

In the present paper, a number of 100 areas has been assumed as a good trade off between accurate results and computational cost. As a consequence, 100 cyclic curves have been adopting in modeling the notch-tip hardening behavior. The linear elastic trend has been maintained constant.

4.2. Example: evaluation of an intermediate curve.

For example, if its needed to assign a curve to a point where the shear stress is 50% of the maximum shear stress the next steps should be followed:

1) Evaluation of K' and n' of the curve from the functions mentioned above:

$$K' = 1510e^{0.0198(\tau\%)}$$

$$n' = 0.0031(\tau\%) + 0.2754$$

Since $\tau\%$ is 50:

$$K'=4063$$

$$n'=0.4304$$

So, the function of the curve associated with a $\tau\%=50$ is:

$$\sigma=4063\varepsilon^{0.4303}$$

Working with Von Mises ranges it becomes:

$$\Delta\sigma_{eq}=4063\Delta\varepsilon_{eq}^{0.4303}$$

Fig. 4.8 shows the curve calculated with this method.

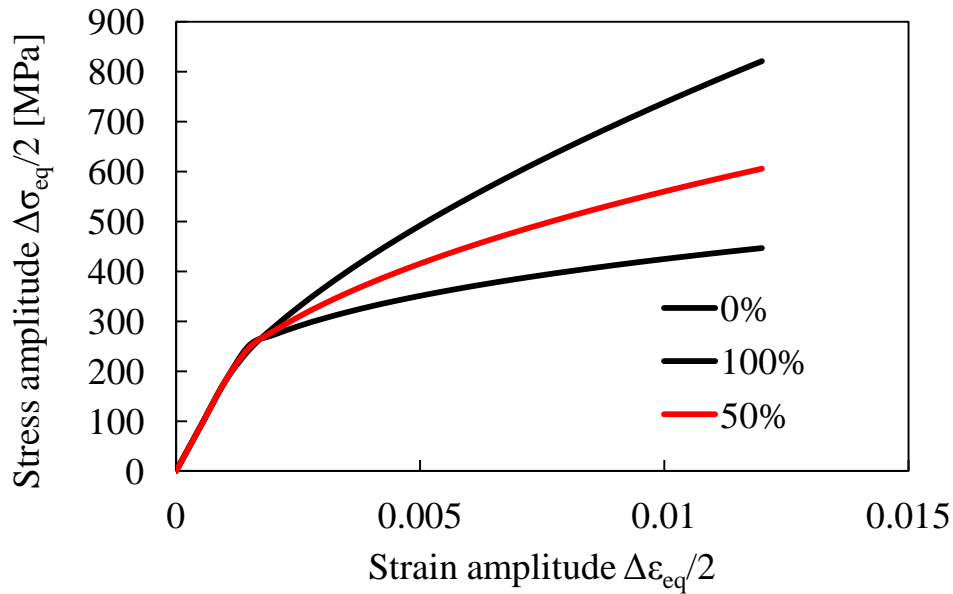


Fig 4.8 Example of curve obtainable by equations (16) and (17) (50% case)

As previously said, it was possible to obtain all the curves for each shear stress percentage.

4.3. Size and shape of areas

To create areas with different value of hardness into the specimen it has been applied the following procedure. Since the model creation is based on shear stress variation in percentage values from push-pull to circle, it's obvious that the variation of this parameter has to be known. Since this variation depends on $K_{t,n}$, a simple torsion load has been applied to all the specimens and the variation of shear stress in percentage values has been obtained along the section (Fig. 4.9). Variation is different depending on notch root radius, and affects the thickness of the areas and their position from the tip (Fig. 4.10).

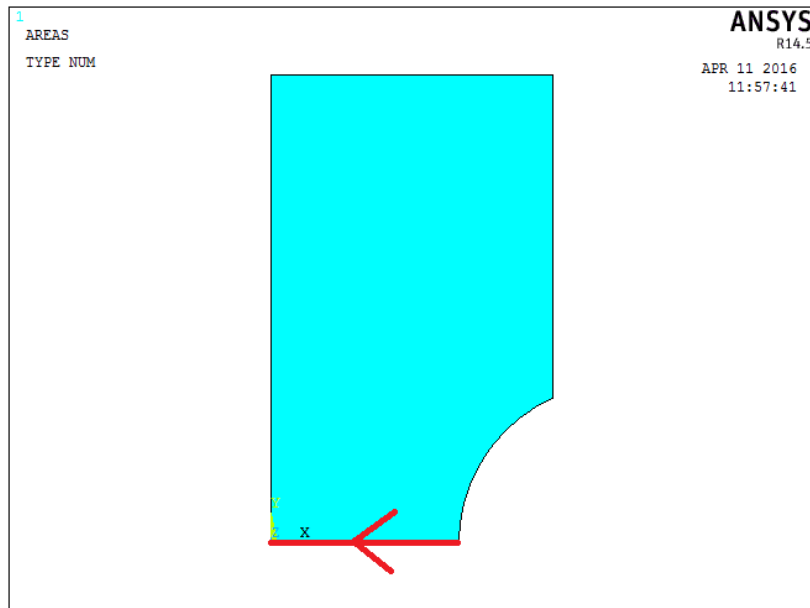


Fig 4.9 Evaluated path for shear stress variation (red line).

Smaller areas, relatively close to each other, have been modeled for high variation of the shear stress, while bigger areas relatively far from each other for small variation.

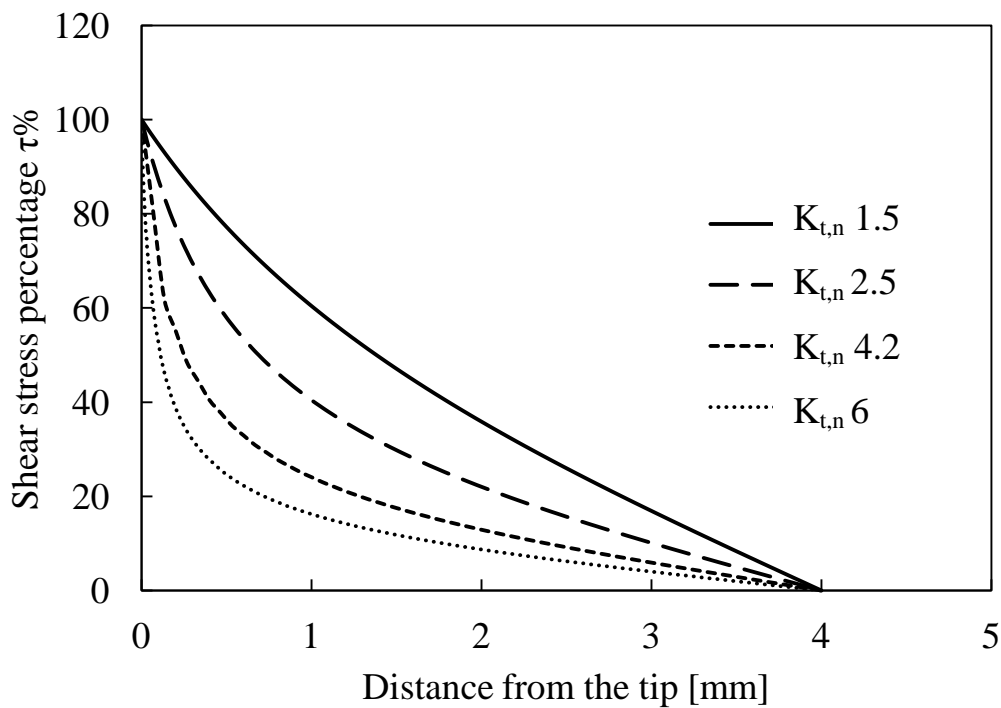


Fig. 4.10 Shear stress variation for different $K_{t,n}$ in percentage values.

It was possible to divide this line in segments each of which correspond to a variation of 1% of shear stress. To simplify the process, a 10% variation was taken and divided in 10 segments. Since the areas are needed and only a line can be divided, areas have been shaped as circles, based on the line division as shown in Fig. 4.11.

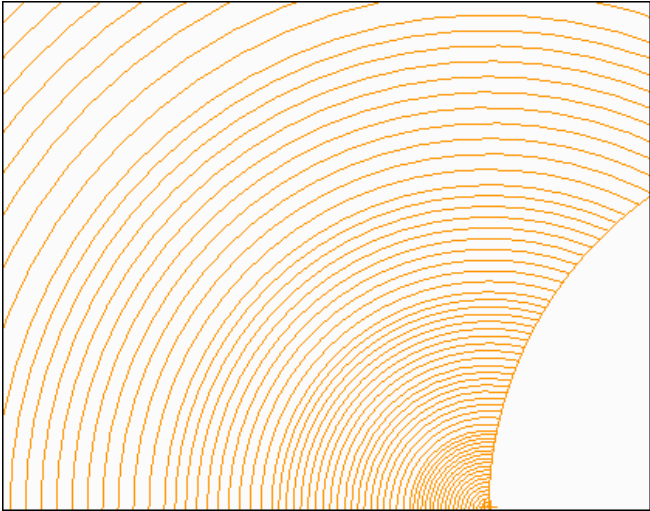


Fig 4.11. Example of areas for K_t 2.5

This is a method to simplify the model, since real shape of areas with different hardness is complicated as shown in Fig. 2.8.

5. SPECIMEN FEM ANALYSIS

This chapter is focused on FEA and all its steps which leads to the evaluation of local maximum strain and K_t' .

5.1. Specimen Geometry

Only a portion of the specimen has been modeled because of its symmetry. The specimen has been created as a 2D plate to simplify the modeling process (Fig 5.1).

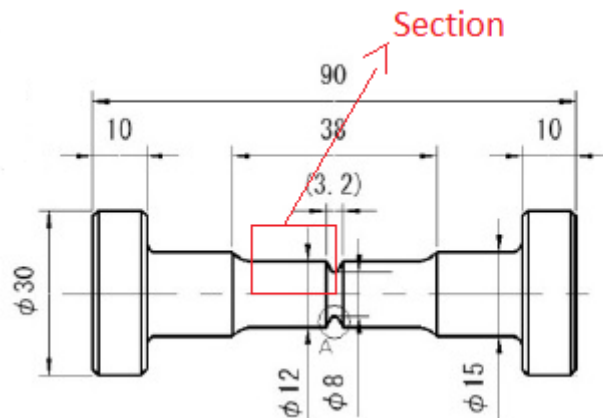


Fig 5.1 Modeled section of the specimen

3D properties has been given successively, by assigning an element which considers axial-symmetry. The geometry changed from a specimen to another because of different notch radius.

Specimen's geometry has been created with the software CREO PARAMETRIC and successively imported in ANSYS.

Global geometry of the specimens is shown in Fig. 5.2 (a,b). For sake of brevity only 2 geometries are reported.

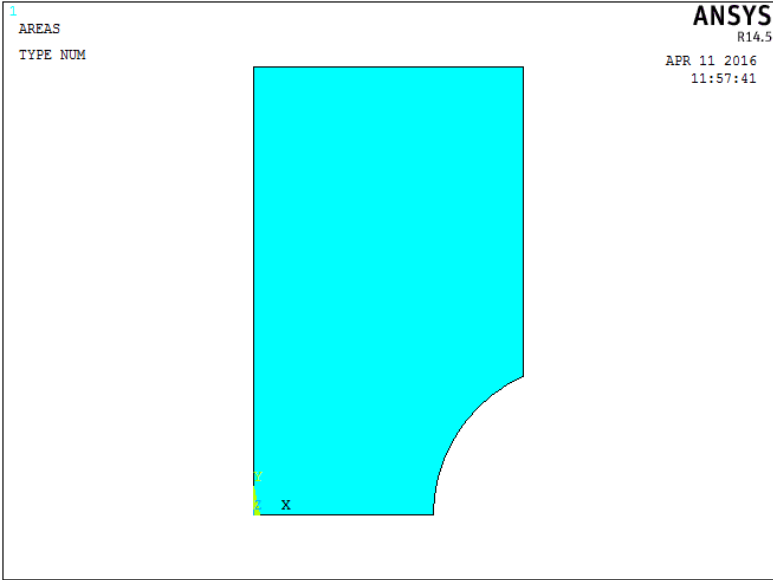


Fig 5.2 (a) $K_{t,n}$ 1.5

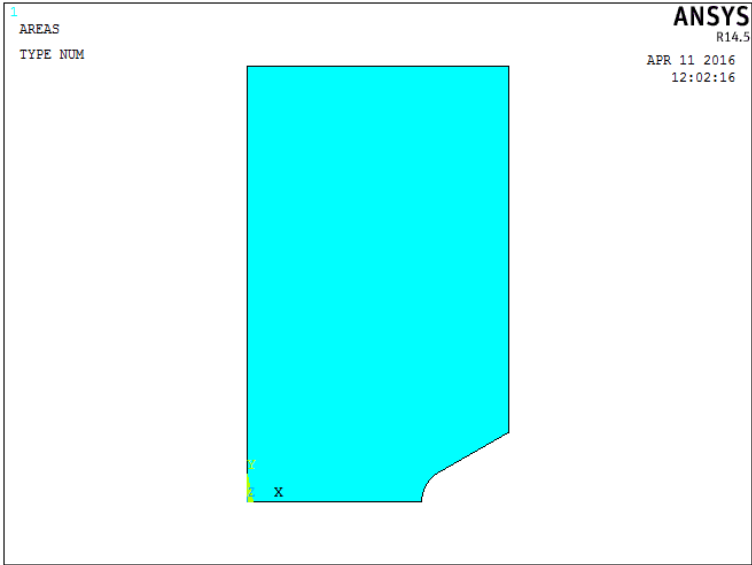


Fig 5.2 (b) $K_{t,n}$ 2.5

5.2. Creation of areas

As explained in previous chapters, the section must be divided following the shear stress tendency to assign the different material constitutive equations. For this reason, a shear stress variation of 10% and the relative length where this variation occurs have been considered. Subsequently, this length has been divided by 10 in order to create 10 lines for every 10% shear stress variation.

This procedure has been applied to simplify the modeling process. The final geometry of the specimen is shown in Fig 5.3

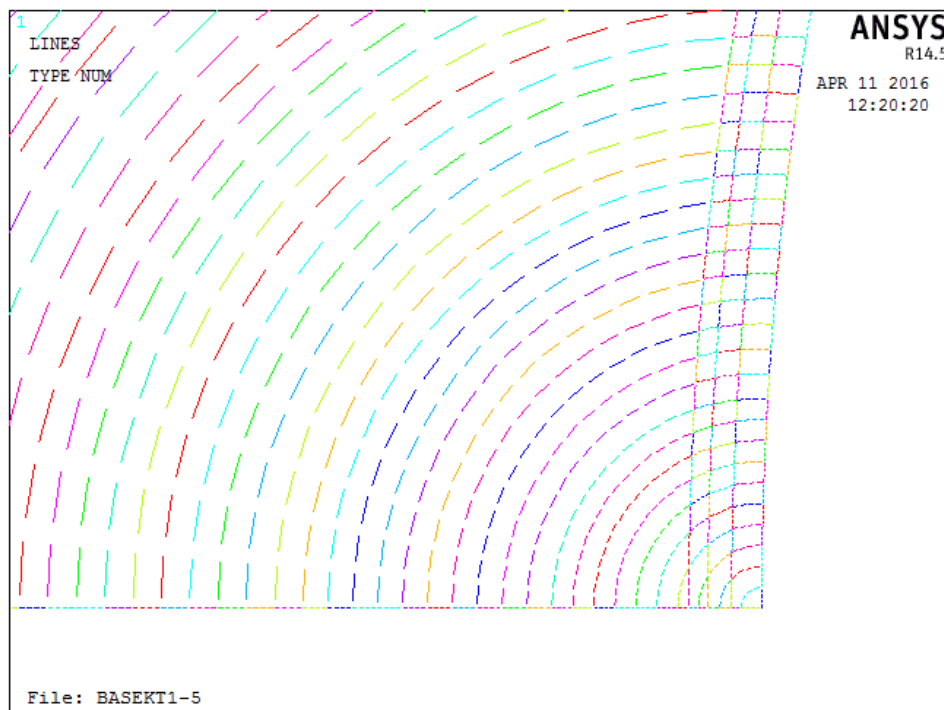


Fig 5.3 Example of areas created from line division ($K_{t,n}$ 1.5)

The divided line based on shear stress variation is the one at the base of the specimen. After this division, a circular segment was created for each shear stress percentage variation of 1% as shown.

5.3. Element type

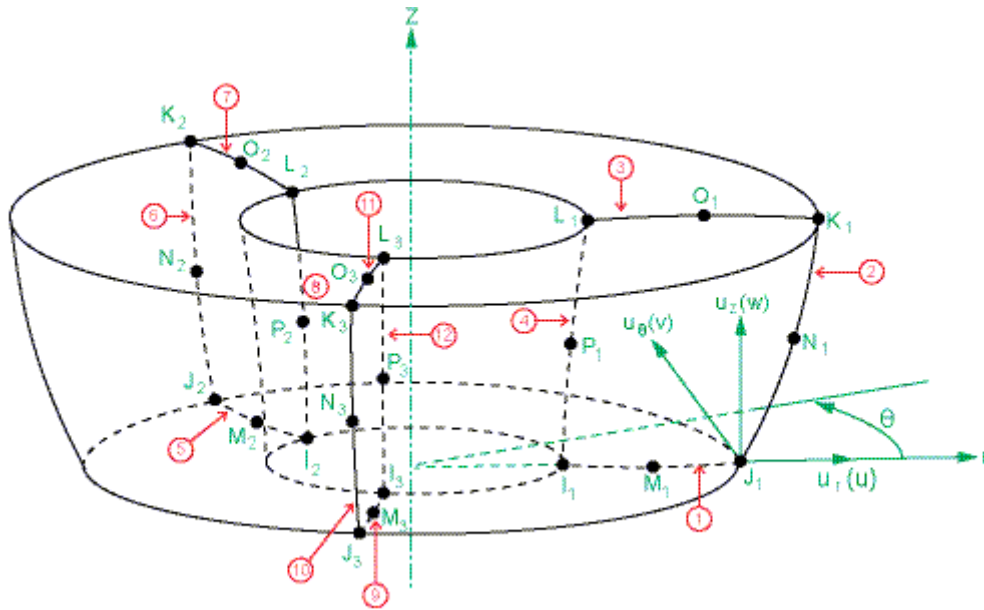


Fig 5.4 Element Solid273 with axisymmetric option

The element has quadratic displacement behavior on the master plane and is well suited to modeling irregular meshes on the master plane. It is defined by eight nodes on the master plane, and nodes created automatically in the circumferential direction based on the eight master plane nodes. The total number of nodes depends on the number of nodal planes (KEYOPT(2)). Each node has three degrees of freedom: translations in the nodal x, y and z directions. The element allows a triangle as the degenerated shape on the base plane to simulate irregular areas. The element has plasticity, hyperelasticity, stress stiffening, large deflection, and large strain capabilities. The default element coordinate system is the cylindrical coordinate system with the Z axis as the axisymmetric axis and the circumferential direction as θ . However, in the simulation the Y axis is taken defined with the command Section in Preprocessor.

This element was chosen because it is an axisymmetric element which allows inelastic analysis and, since LCF is simulated in this analysis, plastic behavior is expected. All the steps for element selection and options are shown in Fig 5.5, 5.6, 5.7.

Preprocessor -> Element Type -> Add/Edit/Delete -> Add
Select Solid and then Solid273:

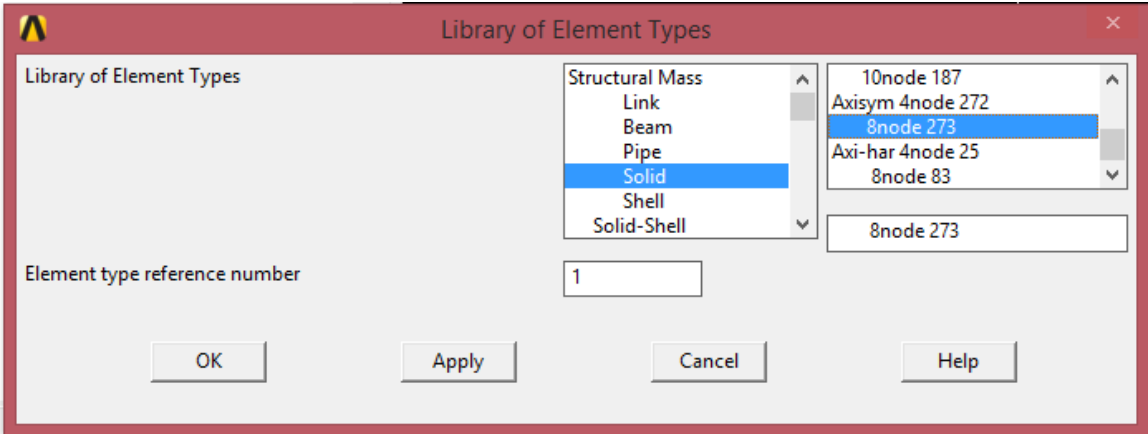


Fig 5.5 Element selection

After the element has been selected, the definition of the Key Option is needed:

Preprocessor -> Element Type -> Add/Edit/Delete.

Select Solid273 previously defined and on the K2 option select axisymmetric on the scroll down menu:

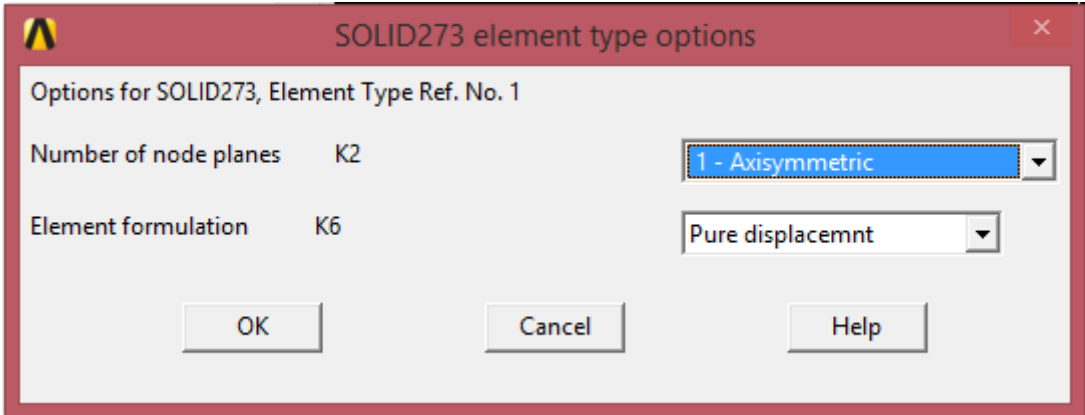


Fig 5.6 Option for axisymmetric

Preprocessor -> Section -> Axis ->Add

After giving an ID to the axis (in this case ID=1) the axis is defined giving in input 2 points (there are other methods for defining the axis). The program asks to insert the two points coordinates which define the axis.

In this case, since Y axis as axisymmetric axis is required, the coordinates are:

P1: $x=0, y=0, z=0$

P2: $x=0, y=20, z=0$

$Y=20$ is a random value. The axisymmetric axis is longer than the specimen's axis so it's sure that the latter is included in the former.

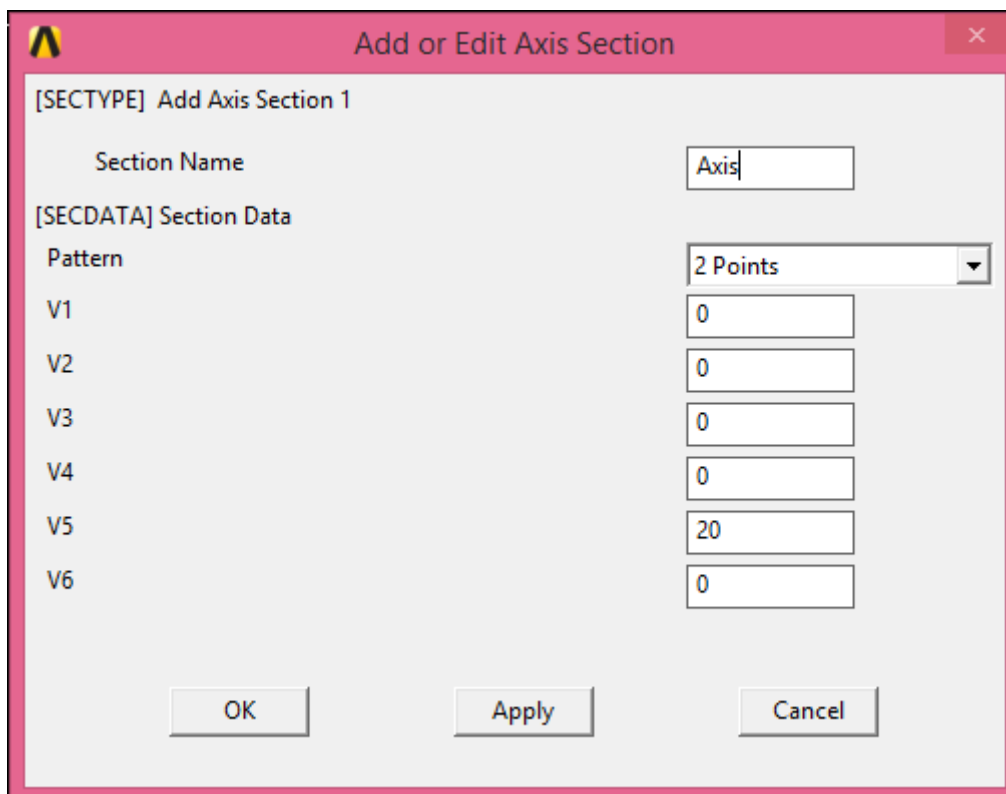


Fig 5.7 Axis definition

In this case: $V1=X1, V2=Y1, V3=Z1, V4=X2, V5=Y2, V6=Z2$

At the end of this process, the element for meshing the model was correctly defined with the axisymmetric axis fixed on cartesian Y axis.

The result of the application of this element is shown in Fig 5.8

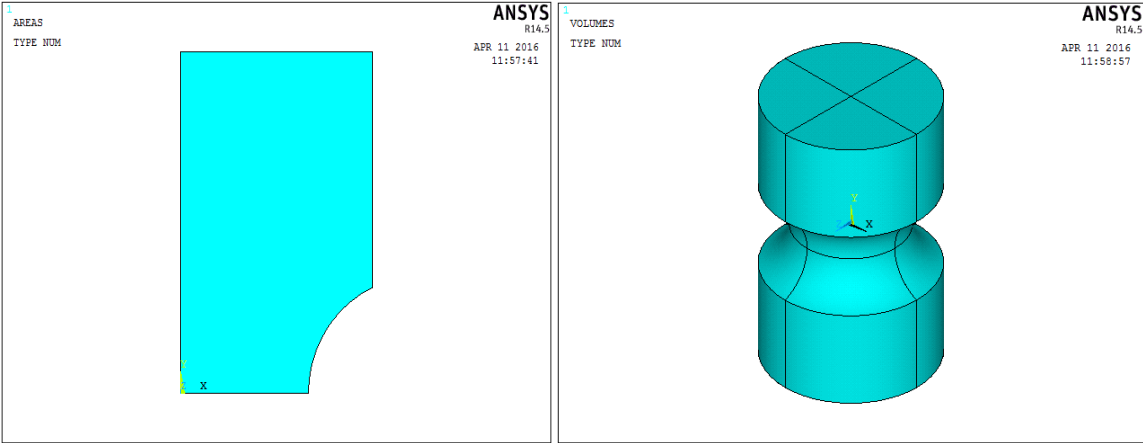


Fig. 5.8 2D model and 3D model ($K_{t,n}$ 1.5)

5.4. Material properties

In order to define the material, a MISO table has been defined.

MISO stands for Multilinear Isotropic and it found a good application if the material has a plastic type curve which defines it. Starting from the curves obtained with the method described in the previous chapters, it has been necessary to insert many points in this table. The program evaluates and plots the curve based on the input points. Since the number of curve to insert is high (100), an APDL file was needed.

After the file has been read, 100 materials were stored in material library, ready to be selected for meshing the different areas based on hardening (Fig 5.9).

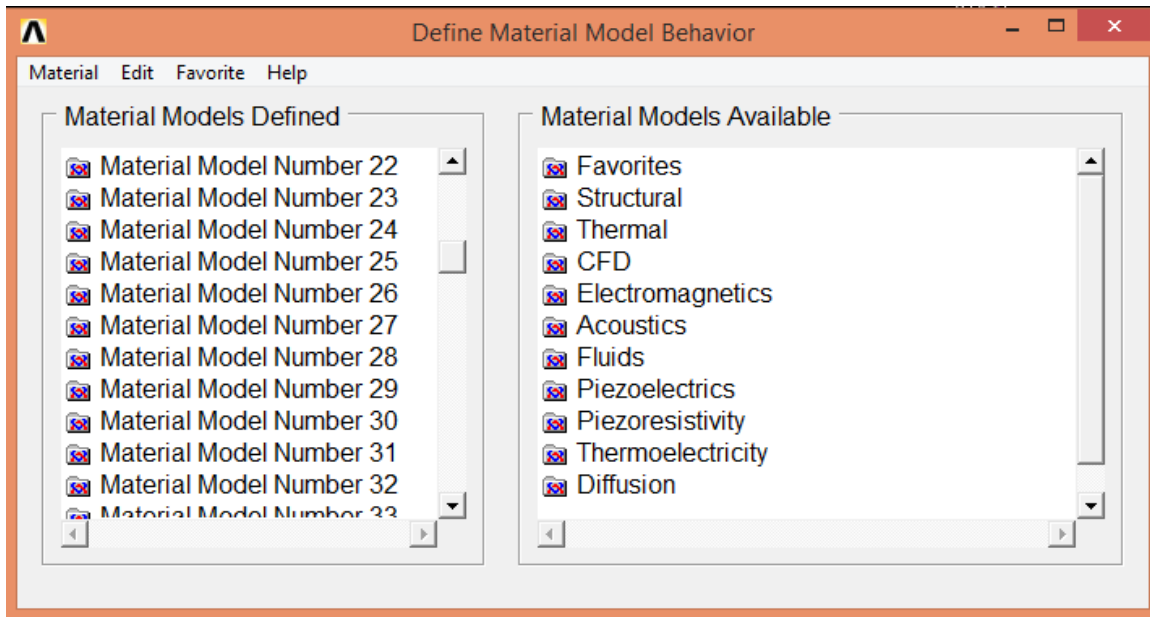


Fig. 5.9 Material library with all the curves

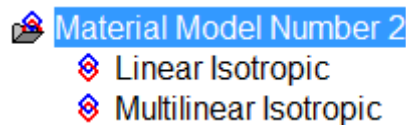


Fig 5.10 Elastic and plastic behavior typical of each curve

Each material has 2 components (Fig 5.10):

- 1) Linear, which describes elasticity
- 2) MISO, which describes plasticity

Linear Isotropic behavior is the same for all the materials since it's an hypothesis under which all the curves have been obtained. Plastic behavior changes since the curves are different. The element is the same (SOLID273) but the material changes. In order to choose the element size, two factor has been taken into account:

- 1) Accuracy in results
- 2) Simulation duration

The element size has been chosen by taking into account that the 2D model corresponds to an axisymmetric model, since the element SOLID273 allows to create from a 2D model in the X-Y plane, a cylindrical model. The most important part to be accurately modeled is the one near the notch tip since the main objective of this work is to evaluate the local maximum strain range, which is located most likely at the tip or nearby it.

5.5. Mesh

The lines were divided using the command

Meshing --> SizeCtrls --> Lines --> Picked Lines

The mesh was created as a free mesh after the definition of areas through the lines. As said, the most important part was the path along the notch border because most probably the maximum strain range was located near the tip. Element size for meshing was an arbitrary choice and it was not a critical parameter because in this case stress concentration factor value is relatively low compared to a crack or a sharp notch. In this case element size depended on $K_{t,n}$. In $K_{t,n}$ 1.5 element size around the tip (most critical point) was higher than in $K_{t,n}$ 6 because of higher variation on stress around it. Giving some values, the element size around the tip in $K_{t,n}$ 1.5 is $7\mu\text{m}$ while in $K_{t,n}$ 6 is $0.25\mu\text{m}$. In the following pictures is shown the mesh near the tip which is the most important place (Fig 5.11 a-d).

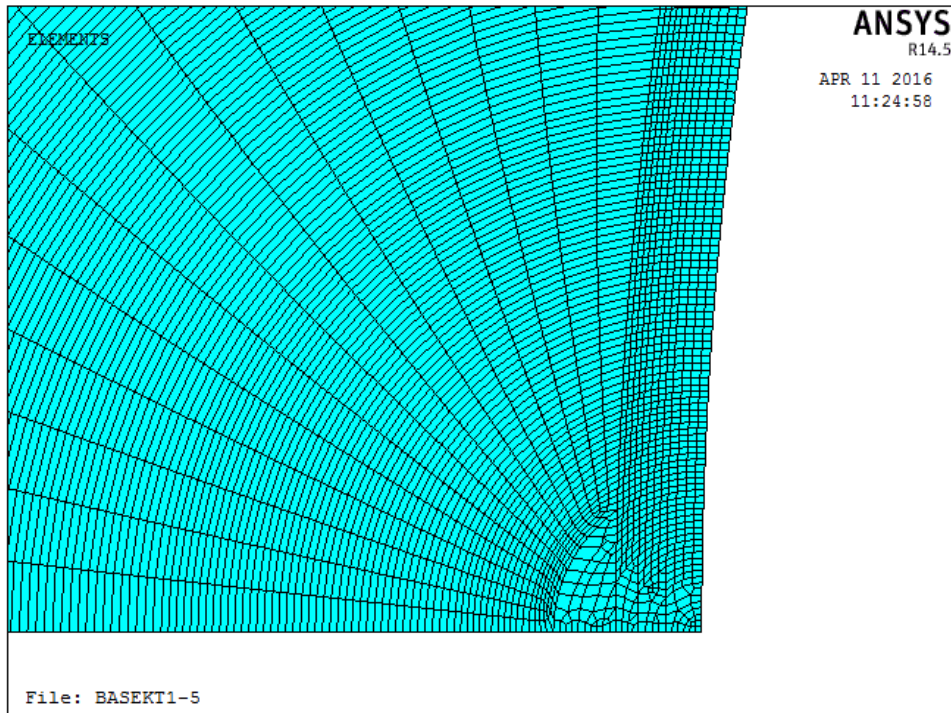


Fig 5.11 (a) $K_{t,n}$ 1.5

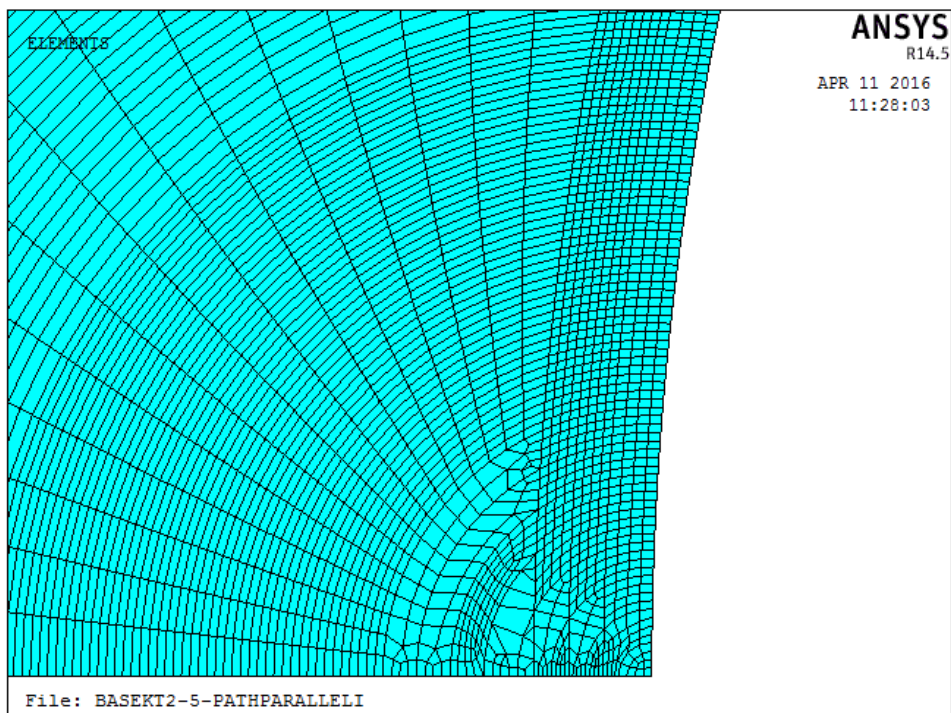


Fig 5.11 (b) $K_{t,n}$ 2.5

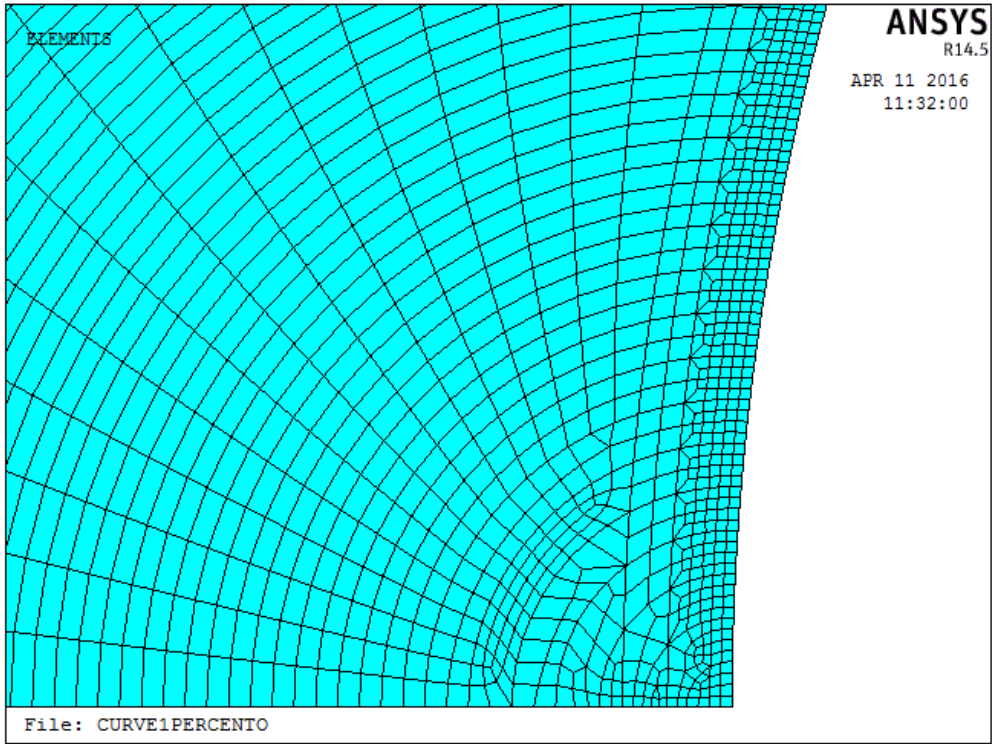


Fig 5.11 (c) $K_{t,n}$ 4.2

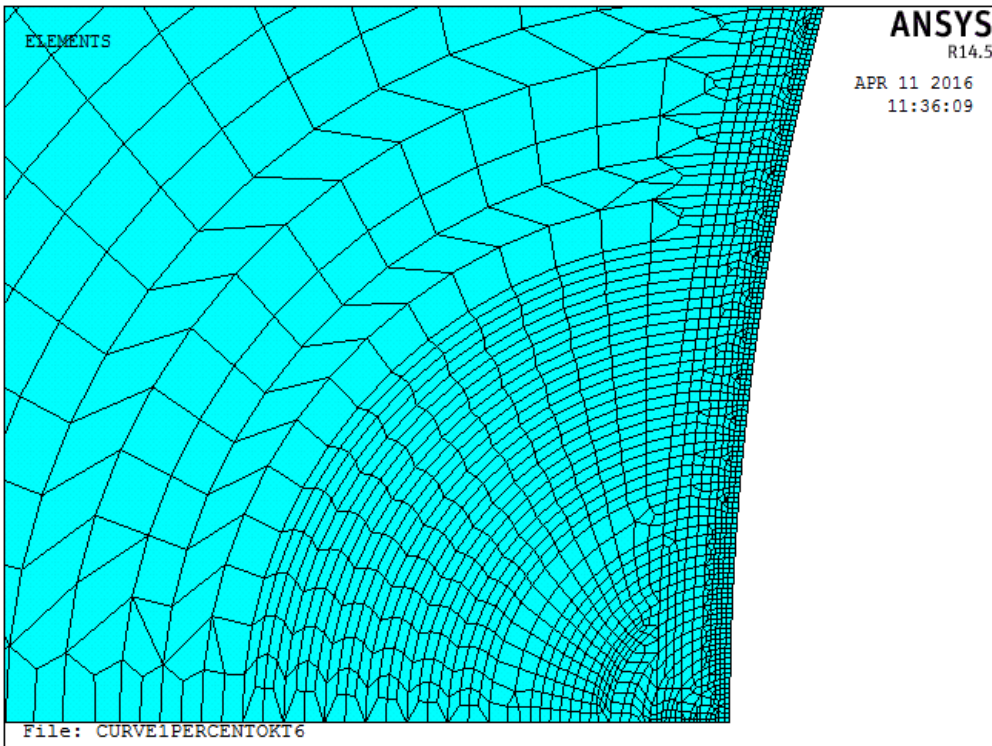


Fig 5.11 (d) $K_{t,n}$ 6

After the APDL file was imported, the number of materials in database was equal to 100 and whenever an area had to be meshed, a new material must have been selected as shown in Fig. 5.12. Different colours represent a different curve (and so a different hardness) which decreases the more is the distance from the tip. Whenever the material changes means that the assigned curve is associated with a decreasing of 1% in shear stress. The final result was a new simplified hardness map that has been tested with a pull test and the results has been acquired based on this model.

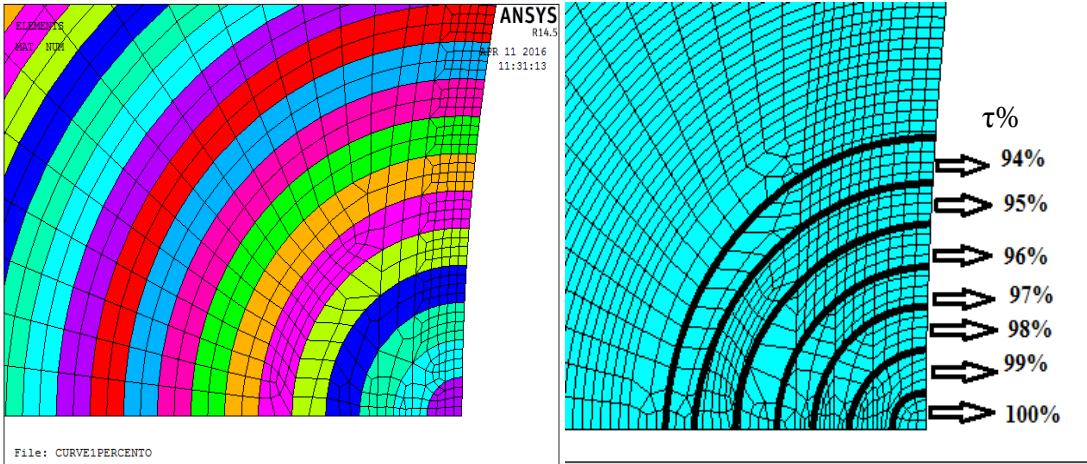


Fig 5.12 Areas with different materials associated to a different curve. Percentage values represent the curve associated to a shear stress percentage.

5.6. Simulation Conditions

Displacements has been set in order to simulate a simple push test. Since the 2D model is only a part of the specimen, symmetry displacements has been applied at the base line of the specimen to take into account the symmetry on X axis. On axisymmetric axis, UX and UY has been applied to simulate a push test. Pressure has been applied to the upper line which value was taken by following the LCF tests made on the specimens (Table 2).

Table 2 Applied loads for circle load cycle

Strain Path	$K_{t,n}$	$\Delta\sigma$ at 1/2 N_f (MPa)	$\Delta\tau$ at 1/2 N_f (MPa)	N_f
Push-Pull	1	680	-	6909
	1.5	800	-	2237
	2.5	800	-	871
	4.2	810	-	571
	6	830	-	418
Circle	1	780	1050	2082
	1.5	850	1030	2248
	2.5	880	1080	475
	4.2	900	1140	212
	6	850	930	156
Reverse	1	-	600	Run Out
	1.5	-	720	54809
	2.5	-	910	4806
Torsion	4.2	-	890	3094
	6	-	850	2243

Since the stress is given as a range, the applied pressure is

$$P = \frac{\Delta\sigma}{2}$$

Since the analysis is non-linear, the simulation parameter has to be set with this procedure:

Solution--> Analysis Type --> Solution Controls

The window to set the analysis parameters is shown in Fig 5.11.

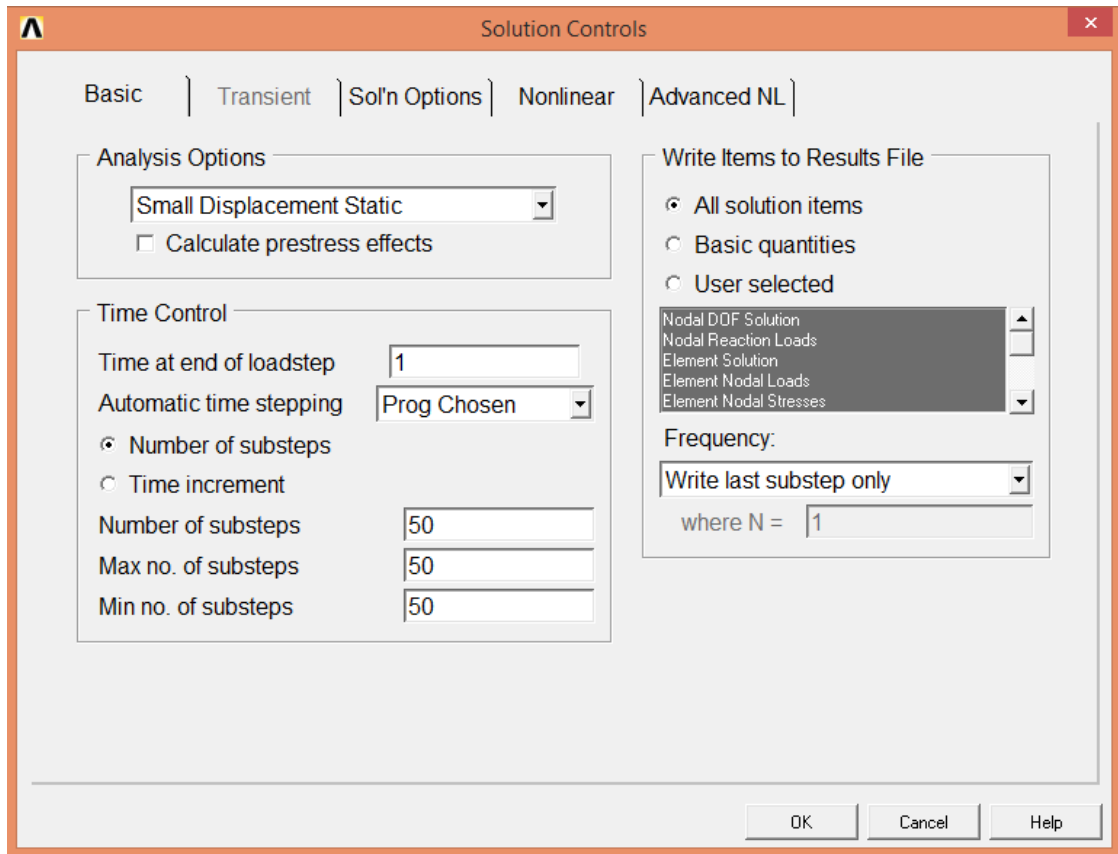


Fig 5.11 Windows for setting analysis conditions

Number of substeps was set on 50 and only the last substep is analysed since there is not cyclic loading applied and the intermediate steps are not taken into account.

6. RESULTS AND DISCUSSION

Local parameters of strain (tangential strain) and stress (Von Mises' Stress) have been obtained through the finite element simulations presented previously.

The contour plots show that the local maximum strain is not at the tip and the maximum equivalent stress is always at the tip. This is due to the different hardness which occurs in the specimen as the result of a LCF test. Since the specimen has not one mechanical behavior but many (given by different hardness), maximum strain is the result of a combination between stress and hardeness. If the specimen would have been modeled with only one curve, maximum strain would have been obviously at the tip since the maximum stress is at the tip. Therefore, since the curve is monotonic, maximum strain would occur in the place where maximum stress is. However, since the curves are many and different, maximum strain is the result of a combination between stress and material hardness. The main result of this simulation is that the maximum strain is not located at the notch tip but at a certain distance from the tip. This value depends on $K_{t,n}$. The area has been modeled following the shear stress variation for each specimen and since the curves are the same for each specimen as hypothesized in the previous chapter, position of maximum strain depends on shear stress variation. The higher is the stress concentration factor, the less is the distance of maximum strain from the tip.

6.1. Stress and strain distribution at the notch root

Contour plots show the values of strain and stress for all specimens Fig. 6.1 (a-d) for strain and Fig. 6.2 (a-d) for stress.

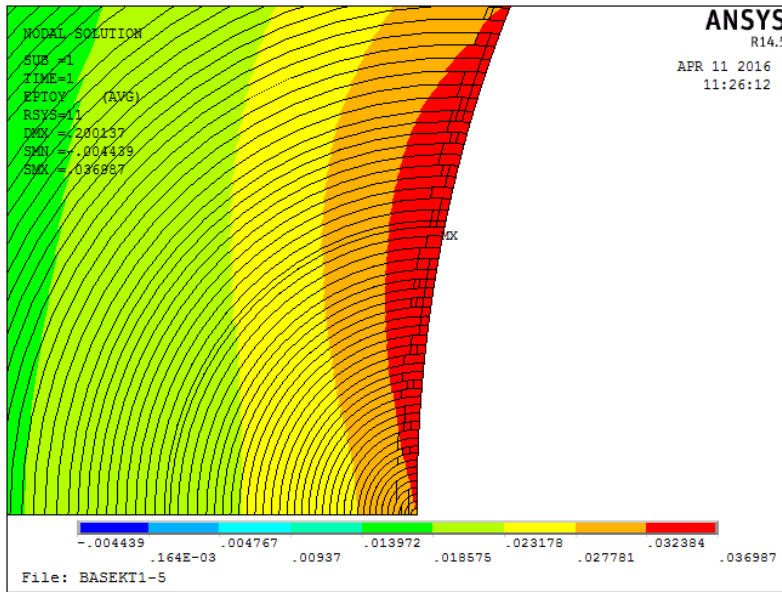


Fig.6.1 (a) Contour plot $\epsilon_0 K_t 1.5$

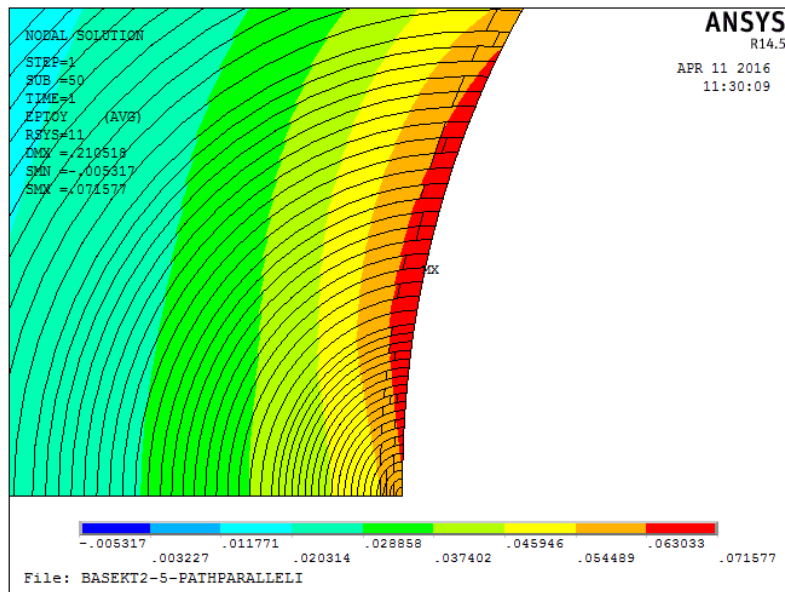


Fig 6.1 (b) Contour plot $\epsilon_0 K_{t,n} 2.5$

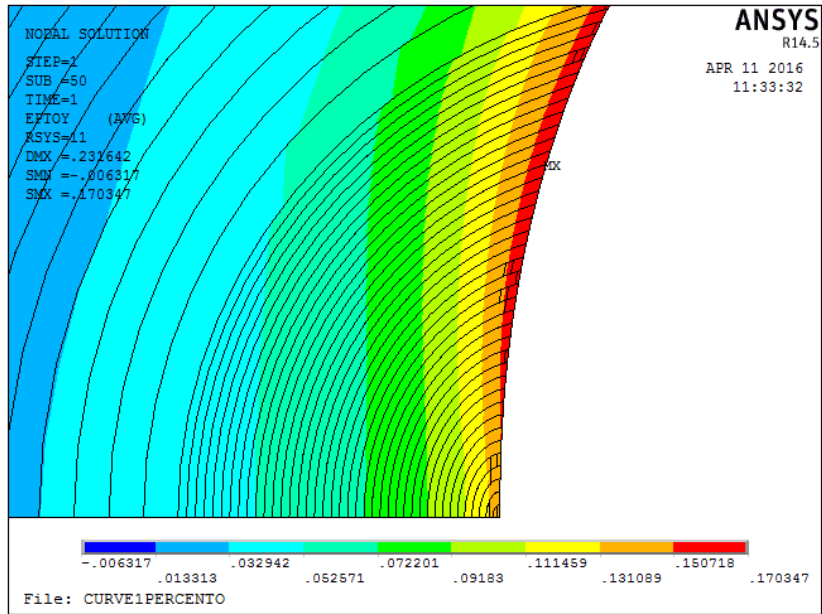


Fig. 6.1 (c) Contour plot $\epsilon_{\theta} K_{t,n} 4.2$

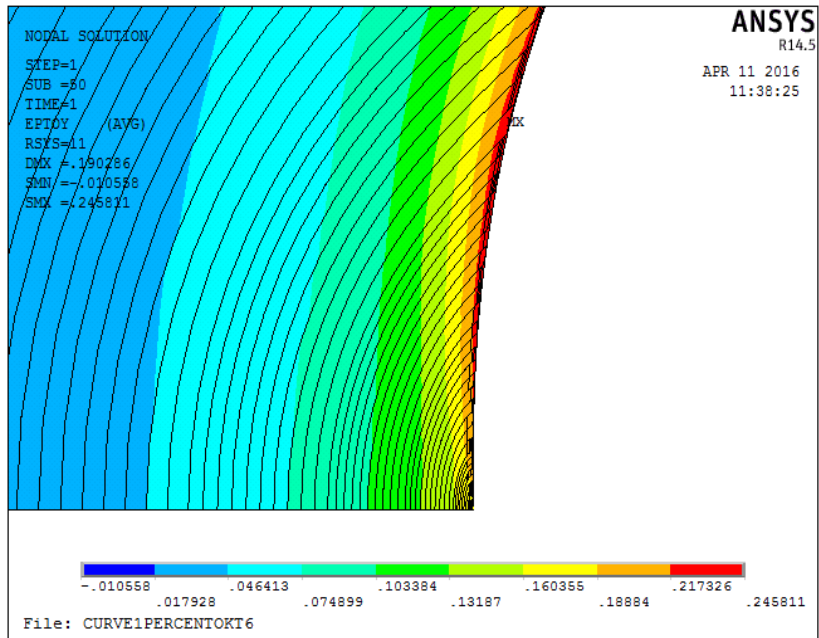


Fig. 6.1 (d) Contour plot $\epsilon_{\theta} K_{t,n} 6$

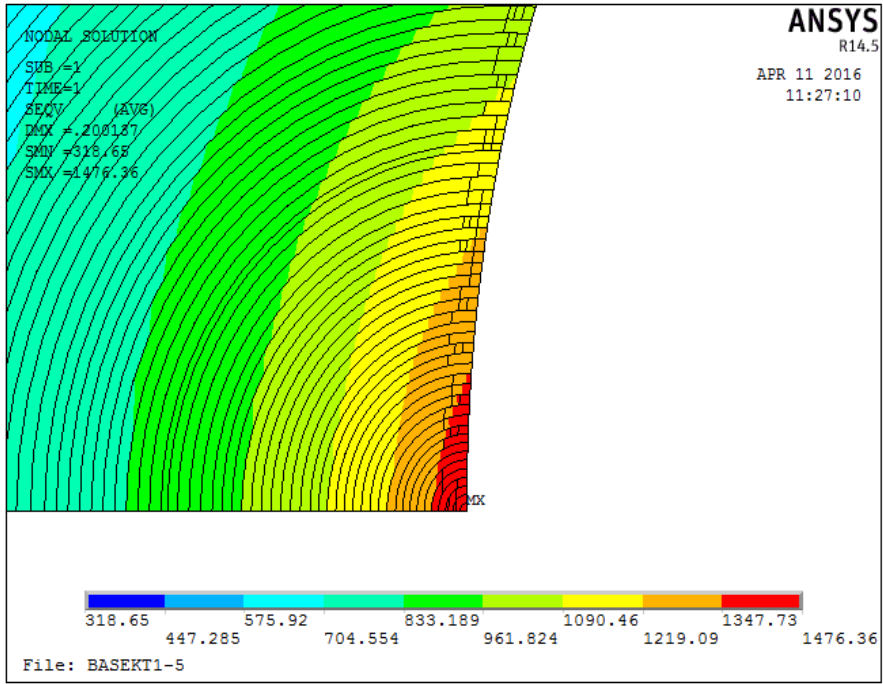


Fig 6.2 (a) Contour plot stress $K_{t,n}$ 1.5

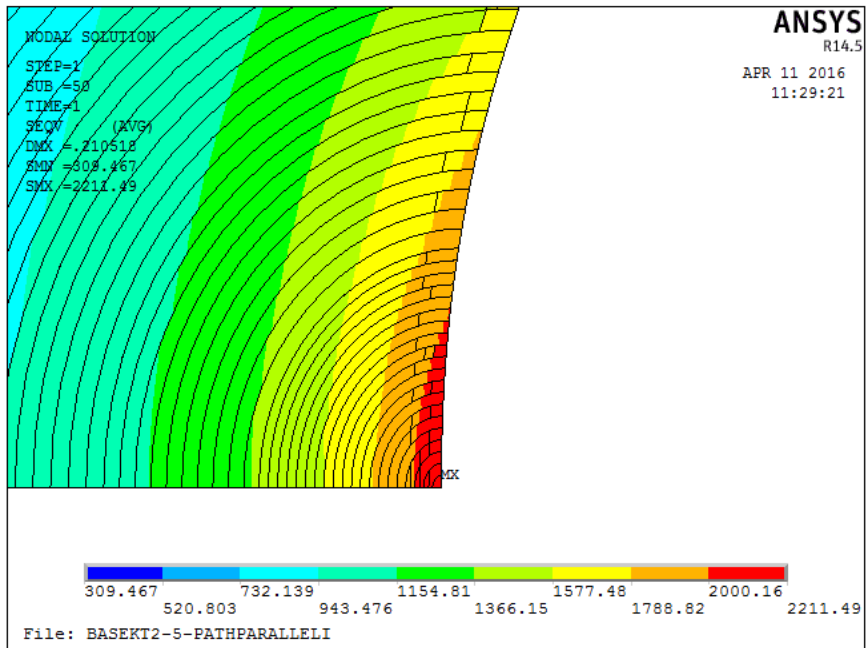


Fig 6.2 (b) Contour plot stress $K_{t,n}$ 2.5

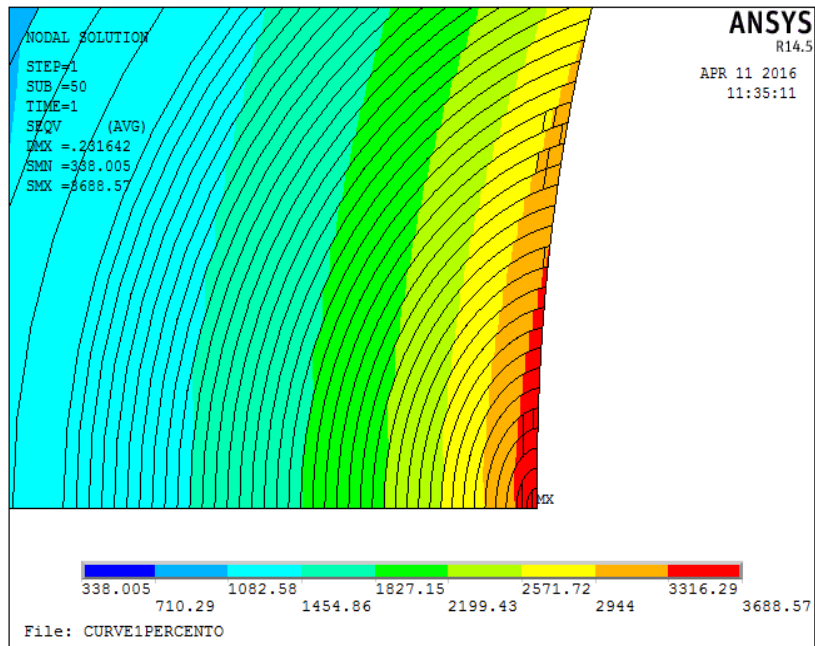


Fig 6.2 (c) Contour plot stress $K_{t,n}$ 4.2

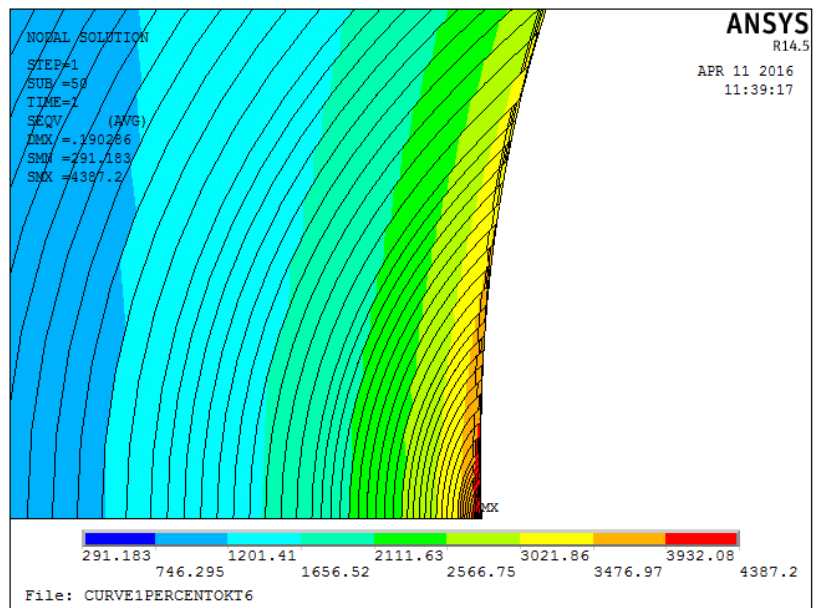


Fig 6.2 (d) Contour plot stress $K_{t,n}$ 6

Maximum value of strain is never located at the tip but is moved from it. The value of this distance depends on $K_{t,n}$ and applied load as said in the previous paragraph. It can be noticed that the colored areas can have some discontinuities. This is due to the resolution of the model given by number of curves which has been chosen for modeling the specimen.

In this case the number of curves is 100 and the resolution employed is acceptable. If the number was lower, discontinuities on plot would have been more evident. On the other hand, with an higher amount of curves, the plot would have been more regular and close to the real behavior of the material but more demanding in terms of time.

The value of distance has been obtained plotting on the path (Fig. 6.3) the maximum strain, shown in Fig 6.4 (a-d). Distance is 0 at the tip and the path follows the red line.

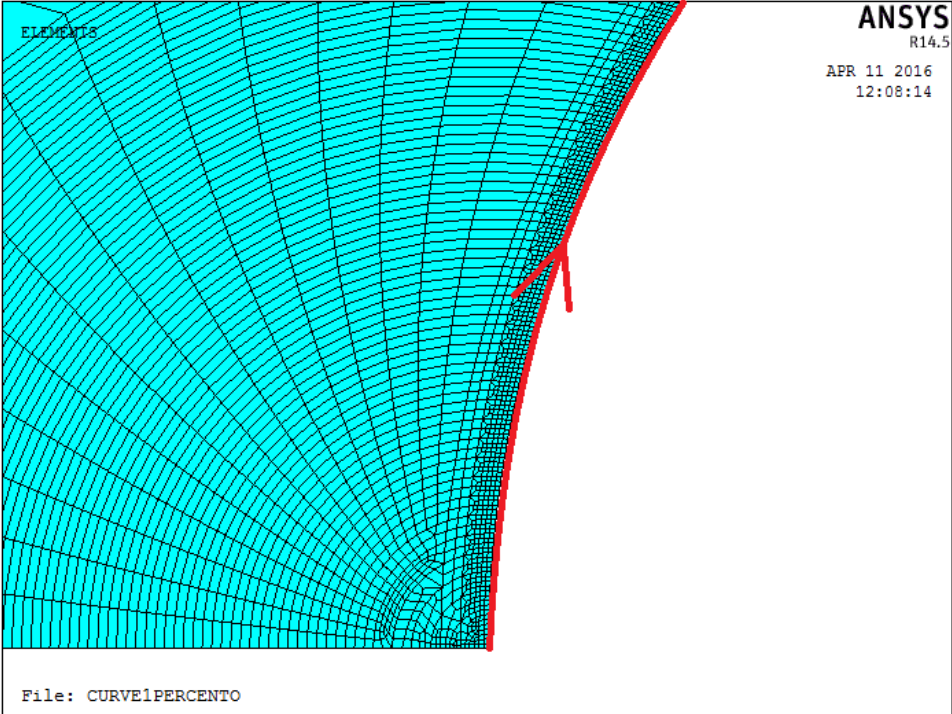


Fig 6.3 Analyzed Path (in red).

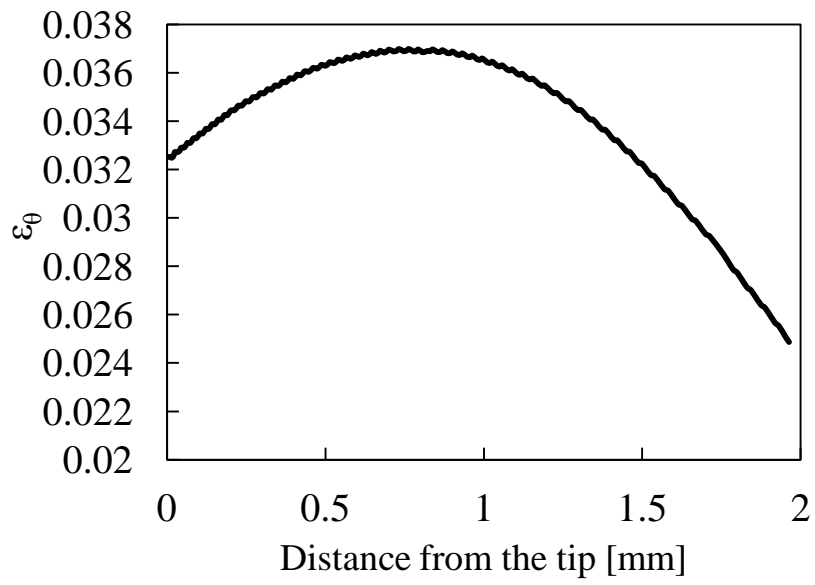


Fig. 6.4 (a) Strain for K_t 1.5

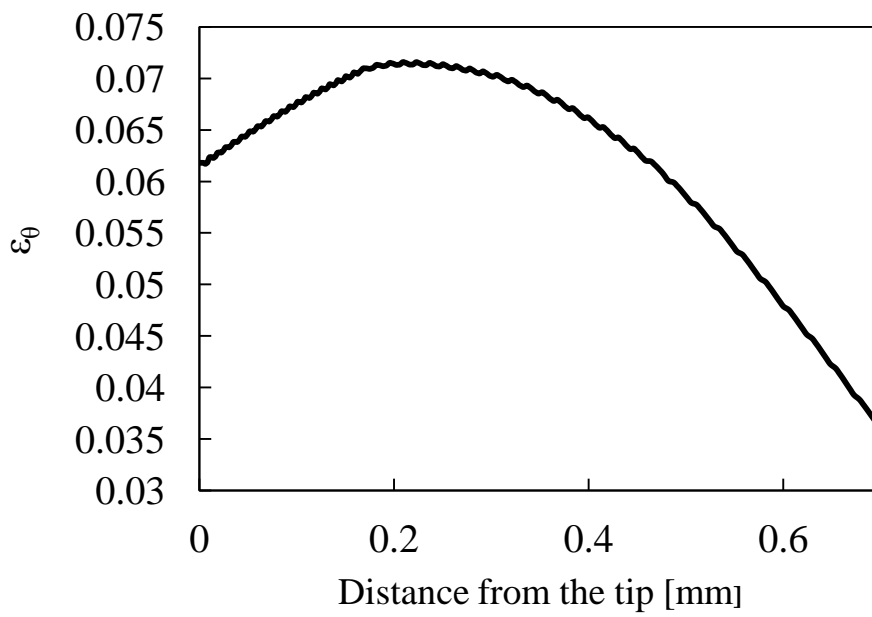


Fig. 6.4 (b) Strain for K_t 2.5

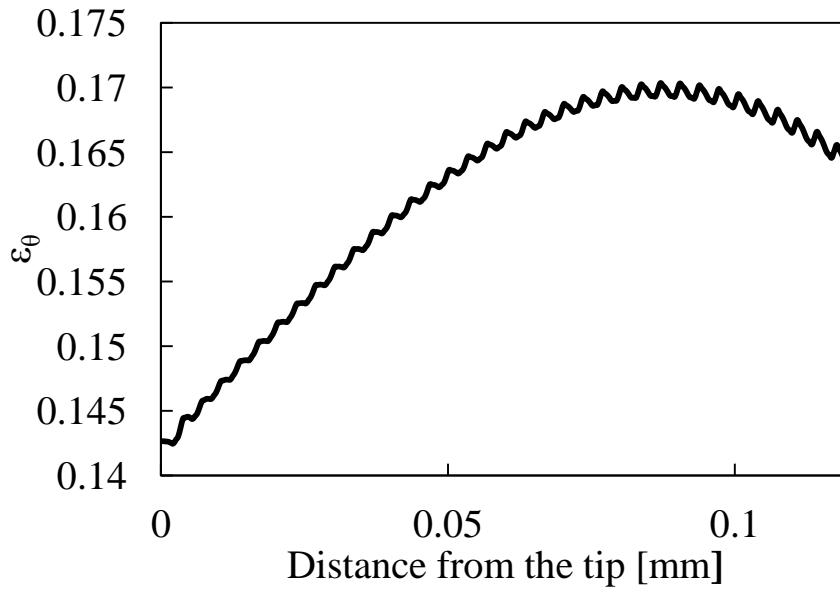


Fig. 6.4 (c) Strain for K_t 4.2

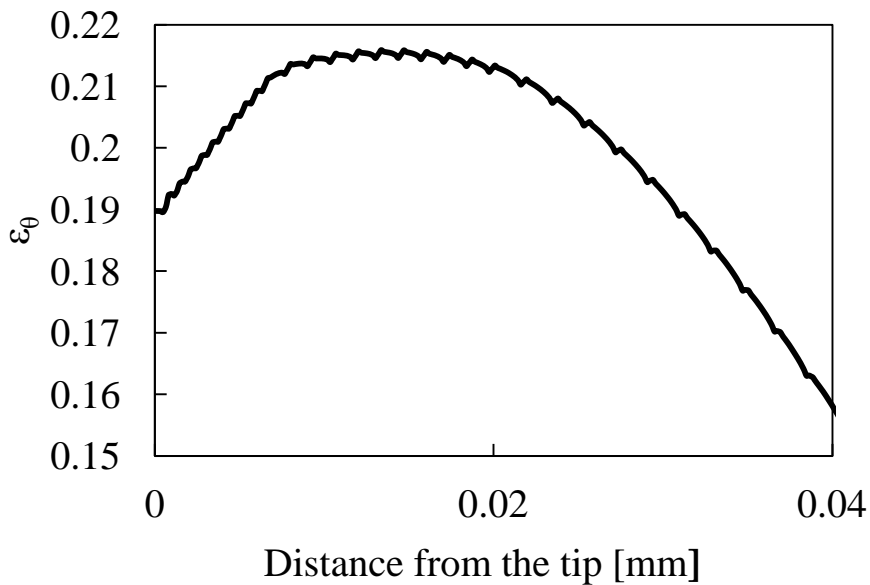


Fig. 6.4 (d) Strain for K_t 6

Discontinuities in the contour plots are evidenced in these graphics. This is due to the resolution of the model: in this case, 100 curves have been used to model the specimen. If an higher number of curves was taken, the line would have been more clear, without fluctuations.

It was necessary to evaluate a new parameter which describes the deflection between the tip and the maximum value of strain. This parameters was evaluated in degrees. First, a center was evaluated according with auxiliary system of curvilinear coordinates defined/employed by Neuber [22] and other authors [23-24]:

$$r_0 = \rho(\pi - 2\alpha)/(2\pi - 2\alpha) \tag{18}$$

Where r_0 is the distance from the notch tip, ρ is the notch root radius and 2α is the notch opening angle (Fig 6.5).

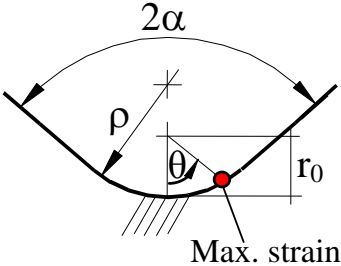


Figure 6.5. Evaluation of the angles within the maximum strain node and the notch root; ρ is the notch radius, 2α is the notch opening angle, distance

$$r_0 = \rho(\pi - 2\alpha)/(2\pi - 2\alpha).$$

After the angle in degrees has been evaluated, it has been divided for $K_{t,n}$ obtaining the angle θ' reported in Table 3. This operation allowed a correct comparison between different geometries.

Table 3. Displacements within the maximum strain node and notch tip root

$K_{t,n}$	ρ (mm)	2α (°)	r_0 (mm)	θ (°)	$\theta'=\theta/K_{t,n}$ (°)
1.5	3.4	48.64	1.44	29.3	19.5
2.5	0.8	60	0.32	37.4	14.9
4.2	0.2	60	0.08	53.4	12.7
6.0	0.09	60	0.036	57.6	9.6

The data summarized in Table 3 gives an explanation about the moved position of the crack initiation spot. The more is the value of $K_{t,n}$, the less is the distance from the notch tip, as shown in Fig 2.9 (Pag. 17).

6.2. Discussion

A comparison has been made using Itoh's model, between local parameters evaluated with FEA and local parameters evaluated with $K_{t,n}$ conventionally defined. Since $K_{t,n}$ is defined as the ratio of local stress and nominal stress in the net section, a new $K_{t,n}$, called K_t' , has been defined. This new parameter was the result of the ratio between stress, located where the maximum strain was (defined in this paper σ'_{loc}), and nominal stress in the net section. Distance of local maximum strain has been evaluated and the value of stress in that point has been carried out. Ratio between this value and nominal stress in the net section has been calculated as K_t' .

$$K_{t,n} = \frac{\sigma_{loc}}{\sigma_n} \quad (19)$$

$$K_t' = \frac{\sigma'_{loc}}{\sigma_n} \quad (20)$$

$$K_t' \Delta \varepsilon_{NP} = K_t' (1 + \alpha f_{NP}) \Delta \varepsilon_1 \quad (21)$$

Obviously K_t' is slightly lower than $K_{t,n}$ conventionally defined since maximum stress is at the tip and σ'_{loc} is located away from the tip (Table 4).

Table 4 $K_{t,n}$ and K_t' values

$K_{t,n}$	K_t'
1.5	1.2
2.5	1.8
4.2	2.8
6	3.4

Figure 6.6 shows the new results obtained. The data are shifted below compared to the results evaluated with conventionally defined K_t .

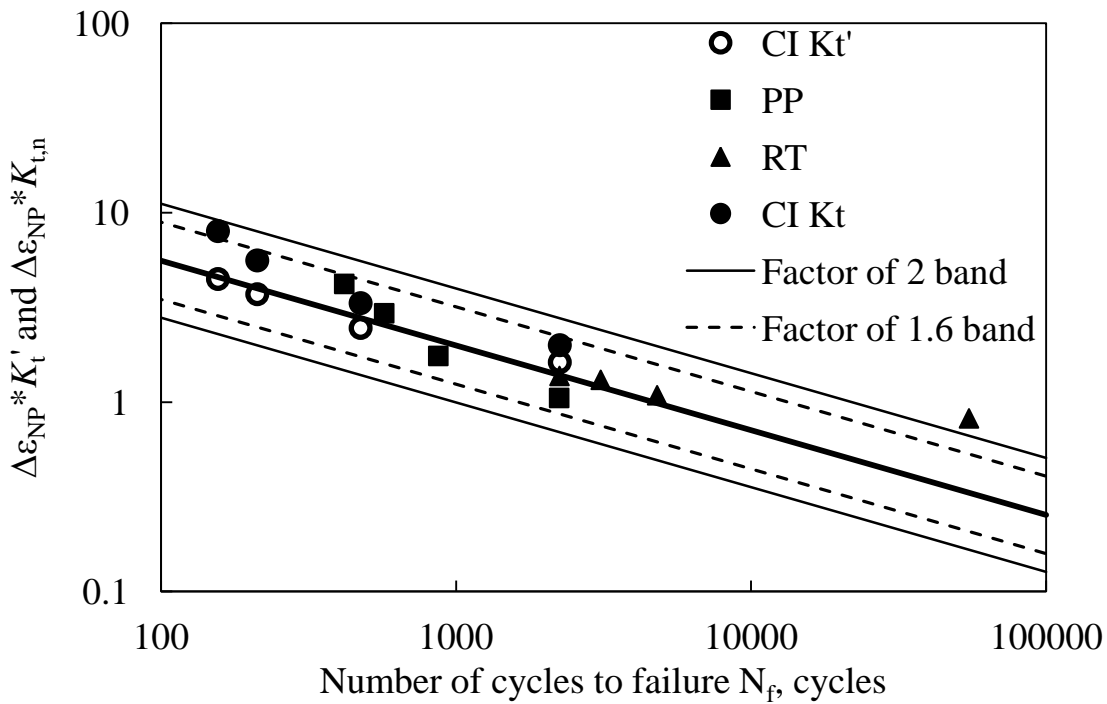


Fig. 6.6 Comparison between $\Delta\epsilon_{np}K_{t,n}$ and $\Delta\epsilon_{np}K_t'$

Results are improved in this interpretation: the data collapse in a factor of 1.6 band, compared to the original data which fit in a factor of 2 scatter band. The factor K_t' takes into account the real behavior of the material by considering the point where the maximum strain is located and, consequently, the spot where crack initiates. This modeling technique considers the real damaging process of

the material and allows to modify the Itoh-Sakane model by improving its accuracy and its interpretation of the real behavior of the material.

7. CONCLUSIONS

The present work presented a new formulation and improvement of the Itoh-Sakane model for multiaxial fatigue under non-proportional loading. On the basis of accurate finite element analysis, taking into account the real hardening behavior of the material, new local parameters have been evaluated and employed in the model. The values have been obtained thank to a sophisticated finite element modeling of the notch tip hardening behaviour. In detail, the specimen was divided in areas to which a specific cyclic curves was assigned, in order to reproduce the real local hardening. This approach, permitted to obtain a notched component with an intrinsic cyclic hardening and a progressive transition within a pure push-pull behaviour occurring at the axis of symmetry (null shear stress) to a circle test at the notch tip (maximum shear stress). A simple tensile load test has been subsequently applied since hardening effect was intrinsically considered in the modeling.

The first result achieved by the present work was to give a non conventional interpretation about multiaxial fatigue simulation, by modeling the specimen as already hardened and by applying a simple axial load, reducing the complexity of the FEA. Otherwise, another option for FEA would have been to give to the material a kinematic hardening rule, which parameters are not always well known, and successively applying a cyclic load. Another goal reached by this work was to show the position of the maximum strain along the notch surface. This result can explain the reason why the crack initiation site is moved from the notch tip, as shown in the tests. This information also allowed to define a different stress concentration factor K_t' , which replaced the originally defined $K_{t,n}$ in Itoh-Sakane model. This substitution made the scatter band more narrow,

allowing to synthesize the relation between strain and fatigue life with more accuracy than the previous results. Furthermore, the results comes from a more realistic interpretation of the material behavior, which other than giving better results for what concerns the scatter band, reflects on the model the true behavior of the material subjected to this particular load cycle.

REFERENCES

- [1] G. Sines, Behaviour of metals under complex stresses, McGraw-Hill, New York, 1959.
- [2] W.N. Findley, A Theory for the Effect of Mean Stress on Fatigue of Metals Under Combined Torsion and Axial Load or Bending, *J. Eng. Ind.* 81 (1959) 301–306.
- [3] H.J. Gough, H. V Pollard, H.J. Gough, The strength of metals under combined alternating stresses, *Proc. Inst. Mech. Eng.* 131 (1935) 3–103.
- [4] M.W. Brown, K.J. Miller, A theory for fatigue failure under multiaxial stress–strain conditions, *Proc. Inst. Mech. Eng.* 187 (1973) 745–755.
- [5] A. Fatemi, D.F. Socie, A critical plane approach to multiaxial fatigue damage including out-of-phase loading, *Fatigue Fract. Eng. Mater. Struct.* 11 (1988) 149–165.
- [6] K.N. Smith, P. Watson, T.H. Topper, Stress-strain function for fatigue of metals, *J. Mater.* 5 (1970) 767–778.
- [7] D.F. Socie, Multiaxial Fatigue Damage Models, *J. Eng. Mater. Technol.*
- [8] K. Liu, A Method Based on Virtual Strain-Energy Parameters for Multiaxial Fatigue Life Prediction, in: *Adv. Multiaxial Fatigue*, ASTM International, 100 Barr Harbor Drive, PO Box C700, West Conshohocken, PA 19428-2959, 1993: pp. 67–67–18.
- [9] G. Rasheda, R. Ghajar, G. Farrahi, Multiaxial stress-strain modeling and effect of additional hardening due to nonproportional loading, *J. Mech. Sci. Technol.* 21 (2007) 1153–1161.
- [10] M. Sakane, T. Itoh, T. Susaki, Y. Kawazoe, Life Prediction for Notched Components in Nonproportional Low Cycle Fatigue: Experiment and FEM Analysis, in: *Press. Vessel Pip. Codes Stand.*, ASME, 2004: pp. 31–38.
- [11] H. Umeda, M. Sakane, M. Ohmani, Notch Root Displacement (NRD) Approach to Predict Crack Initiation Life of Notched Specimen in High-Temperature Multiaxial Low Cycle Fatigue, *J. Eng. Mater. Technol.* 112 (1990) 429–434.
- [12] H. Umeda, M. Sakane, M. Ohnami, Notch Effect in Biaxial Low Cycle Fatigue at Elevated Temperatures, *J. Eng. Mater. Technol.* 111 (1989) 286–293.
- [13] M.E. Barkey, D.F. Socie, K.J. Hsia, A Yield Surface Approach to the Estimation of Notch Strains for Proportional and Nonproportional Cyclic Loading, *J. Eng. Mater. Technol.* 116 (1994) 173.

- [14] A. Savaidis, G. Savaidis, C. Zhang, Elastic–plastic FE analysis of a notched shaft under multiaxial nonproportional synchronous cyclic loading, *Theor. Appl. Fract. Mech.* 36 (2001) 87–97.
- [15] M. Sakane, S. Zhang, T. Kim, Notch effect on multiaxial low cycle fatigue, *Int. J. Fatigue.* 33 (2011) 959–968.
- [16] T. Itoh, T. Nakata, M. Sakane, M. Ohnami, Nonproportional Low Cycle Fatigue of 6061 Aluminum Alloy Under 14 Strain Paths, in: Macha Al., Ed. *Multiaxial Fatigue Fract.*, 1999: pp. 41–54.
- [17] T. Itoh, M. Sakane, M. Ohnami, D.F. Socie, Nonproportional Low Cycle Fatigue Criterion for Type 304 Stainless Steel, *J. Eng. Mater. Technol.* 117 (1995) 285.
- [18] T. Itoh, T. Yang, Material dependence of multiaxial low cycle fatigue lives under non-proportional loading, *Int. J. Fatigue.* 33 (2011) 1025–1031.
- [19] T. Morishita, T. Itoh, M. Sakane, Evaluation and visualization of multiaxial stress and strain states under non-proportional loading, *Frat. Ed Integrità Strutt.* 33 (2015) 289–301.
- [20] T. Itoh, W. Chen, R. Yamamoto, Multiaxial Low Cycle Fatigue Life of Notched Specimen for Type 316L Stainless Steel under Non-Proportional Loading, *J. Solid Mech. Mater. Eng.* 5 (2011) 230–241.
- [21] H. Neuber, Theory of Stress Concentration for Shear-Strained Prismatical Bodies With Arbitrary Nonlinear Stress-Strain Law, *J. Appl. Mech.* 28 (1961) 544.
- [22] H. Neuber, *Theory of Notch Stresses: Principles for Exact Calculation of Strength with Reference to Structural form and Material*, 2nd ed., Springer-Verlag, Berlin, 1958.
- [23] N.I. Muskhelishvili, *Some Basic Problems of the Mathematical Theory of Elasticity*, Leyden, 1953.
- [24] P. Lazzarin, R. Tovo, A unified approach to the evaluation of linear elastic stress fields in the neighborhood of cracks and notches, *International Journal of Fracture.* 78 (1996) 3–19.

ACKNOWLEDGEMENTS

First of all, I would like to thank the members of my family: my father and my mother for supporting me financially in this long educational path and for following me in every choice I made. My brother Edoardo, who has always been an example to follow under both moral and educational point of views.

I would like also to thank the persons who followed me in these six months of work. Professor Filippo Berto, for giving me the opportunity to live an incredible experience and for being always professional and kind towards me. Professor Takamoto Itoh and Takahiro Morishita for hosting me in their laboratory in Ritsumeikan University and for the great patience shown on answering me to my every single request of help. Finally, I would like to thank Dr. Pasquale Gallo for helping me to live better my experience abroad and for constantly following me in my work, not only to make it better but also for making me learn from my mistakes and by doing so, helping me to improve.

I would like also to thank my university friends, in particular Milo and Matteo, for helping me to face my days with a smile and for sharing ignorant moments during all the time i spent in Vicenza.

Special thanks to Alberto for sharing with me five years of my life. Most of the exams, projects, reports we have worked on, they have been a success mostly thanks to him, who has always been a true friend and a beautiful person.

Thanks also to all the friends I met in Japan: Peter, Yugo, Narasaki, Keki, Misato, Alexandre, Alex, Sam, Julien, Rim, Justin, Jack, Rikuto and Ayaka. I shared beautiful moments with them and they will be always in my heart.

Thanks also to all my friends in San Bonifacio: Mox, Pangra, Pelo, Batti, Check, Gimmy e Torn. I spent all my life with them and this result i just achieved will be the chance for them to unchain their hidden fantasies. Please guys be kind . I would also like to thank Rocco for his suggestions about my career and for making me live remarkable moments.

I would also like to thank my scout group San Bonifacio 2 which, in 18 years of experience, made me understand that life not easy sometimes, but successes can always be reached if we face challenges with perseverance and will to dream.

Finally, I want to thank Kazuki. I shared beautiful moments with her. Thank you for helping me to get over bad situations after my return in Italy and for giving me a lot of motivations about chasing goals which seems impossible to reach.

"Paddle your own canoe, don't rely on other people to row your boat.

*You are starting out on an adventurous voyage;
from the stream of childhood, along the river of adolescence,
out across the river of manhood to the port you want to reach.*

You will meet difficulties and dangers, shoals and storms on the way.

But without adventure, life would be deadly dull.

*With careful piloting, above-board sailing, and cheery persistence,
there is no reason why your voyage should not be a complete success;
no matter how small was the stream in which you make your start.*

Sir Robert Baden-Powell, 1992

RINGRAZIAMENTI

Innanzitutto vorrei ringraziare i componenti della mia famiglia: mia madre e mio padre per avermi sostenuto economicamente in questo lungo cammino di formazione scolastica e che mi hanno accompagnato in ogni scelta che ho fatto. Mio fratello Edoardo, che da sempre è stato un esempio da seguire sia dal punto di vista formativo che morale: la maggior parte dei risultati che ho ottenuto li devo a lui.

Ringrazio poi le persone che mi hanno accompagnato in questi ultimi sei mesi di sviluppo di questa tesi di laurea. Il professor Filippo Berto per avermi dato l'opportunità di vivere un'esperienza incredibile e per essersi dimostrato sempre disponibile, professionale e cordiale nei miei confronti. Il professor Takamoto Itoh e Takahiro Morishita per avermi ospitato nel loro laboratorio alla Ritsumeikan University e per la loro grande pazienza nel rispondere con assiduità ad ogni mia singola domanda. Infine ringrazio infinitamente il Dr. Pasquale Gallo per avermi aiutato a vivere la mia esperienza all'estero al meglio e per avermi seguito assiduamente nel mio lavoro, non solo per migliorarlo, ma per avermi anche fatto notare i miei errori, aiutandomi a crescere.

Un grazie a tutte le persone con cui ho condiviso moltissimi momenti in questi anni di università, in particolare Milo e Matteo: il tempo passato assieme mi ha aiutato ad affrontare le mie giornate con un sorriso, vivendo momenti davvero ignoranti nella mia vita a Vicenza.

Volevo ringraziare inoltre Alberto per aver condiviso con me cinque anni della mia vita in università. Gran parte di esami che ho passato, relazioni, progetti, su cui abbiamo lavorato, sono andati a buon fine grazie a lui che si è sempre dimostrato un amico vero ed una bellissima persona.

Un grazie inoltre va a Peter, Yugo, Narasaki, Keki, Misato, Alexandre, Alex, Sam, Julien, Rim, Justin, Jack, Rikuto e Ayaka per avermi fatto vivere momenti stupendi in Giappone e che porterò sempre nel cuore.

Ringrazio anche i miei amici di San Bonifacio Mox, Pangra, Pelo, Batti, Check, Gimmy e Torn. Ho vissuto una vita intera con loro e questo risultato che ho raggiunto sarà un'occasione per loro per scatenare le loro più nascoste fantasie. Siate gentili ragazzi. Un grazie va inoltre a Rocco, che mi dato consigli sulla mia carriera e che mi fa vivere da sempre momenti memorabili.

Ringrazio il gruppo A.G.E.S.C.I San Bonifacio 2, che in ormai 18 anni di esperienza mi ha fatto capire che la vita è sempre una continua sfida, ma che i successi arrivano sempre se affrontata con costanza e voglia di sognare.

Infine, voglio ringraziare Kazuki. Ho condiviso giornate stupende con lei. Grazie per avermi aiutato a superare situazioni difficili dopo il mio ritorno in Italia e per darmi ragioni sempre nuove per continuare a perseguire obiettivi che sembrano impossibili.

*"Guida tu stesso la tua canoa, non contare sull'aiuto degli altri.
Tu parti dal ruscello della fanciullezza per un viaggio avventuroso;
di là passi nel fiume dell'adolescenza;
poi sbocchi nell'oceano della virilità per arrivare al porto che vuoi raggiungere.
Incontrerai sulla tua rotta difficoltà e pericoli, banchi e tempeste.
Ma senza avventura, la vita sarebbe terribilmente monotona.
Se saprai manovrare con cura, navigando con lealtà e gioiosa persistenza, non c'è ragione
perché il tuo viaggio non debba essere un completo successo;
poco importa quanto piccolo fosse il ruscello dal quale un giorno partisti".*

Sir Robert Baden-Powell, 1922